ELSEVIER

Chemical Geology 184 (2002) 311–335

CHEMICAL GEOLOGY
INCLUDING
ISOTOPE GEOSCIENCE

www.elsevier.com/locate/chemgeo

# W- and M-type tetrad effects in REE patterns for water–rock systems in the Tono uranium deposit, central Japan

Yoshio Takahashi [a,*], Hidekazu Yoshida [b,1], Nana Sato [c], Katsuhiro Hama [b], Yasuhisa Yusa [b], Hiroshi Shimizu [a]

[a] *Department of Earth and Planetary Systems Science, Graduate School of Science, Hiroshima University, Higashi-Hiroshima, Hiroshima 739-8526, Japan*

[b] *Tono Geoscience Center, Japan Nuclear Cycle Development Institute (JNC), Toki, Gifu 509-5102, Japan*

[c] *Department of Earth Sciences, Faculty of Science, Kumamoto University, Kumamoto 860-8555, Japan*

Received 15 December 2000; accepted 5 September 2001

**Abstract**

Abundances of rare earth elements plus Y (REE) were determined for granitic rocks, Tertiary sedimentary rocks, and related groundwater in the Tono area, central Japan. Tetrad effects, concave curves in REE patterns, were found for these rocks and groundwater samples. Conjugate M- and W-types of tetrad effects were simultaneously observed in these specimens which constitute the water–rock system; the granitic rocks show the M-type tetrad effects while the groundwater and the sedimentary rocks exhibit the W-type tetrad effects. Non-chondritic Y/Ho ratios were found especially in the groundwater; Y/Ho ratios showed larger values than the chondritic value for the samples showing W-type tetrad effects, and vice versa. These results suggest that: (1) preference of the groundwater for a W-type tetrad effect and larger Y/Ho ratio than chondrite produces an M-type tetrad effects and lower Y/Ho ratios in the granitic rocks during weathering processes; (2) the W-type tetrad effect and larger Y/Ho ratio for the sedimentary rocks is brought about by the fixation of groundwater REE onto the sedimentary rocks. The variation of the tetrad effect and Y/Ho ratio was confirmed by laboratory experiments on the leaching of REE from the granitic rocks. The W-type tetrad effect and large Y/Ho ratio in the U-mineralization zone in the sedimentary rocks were also found by SIMS analysis, which is consistent with the W-type tetrad effect and larger Y/Ho ratio in the whole rock abundances of the sedimentary rocks. Disequilibrium of the U series ($^{234}U/^{238}U$), analyzed by SIMS in the U-mineralization zone, suggests that the U-bearing minerals were formed through precipitation from groundwater as it became reducing. These results suggest that the REE in the sedimentary rocks were transported by the groundwater from the granitic rocks in the Tono area. Based on this study, it is implied that the degree of the tetrad effects and the variation of Y/Ho ratio can be valuable tools to investigate the migration of REE during water–rock interactions in natural systems. 

*Keywords:* Rare earth elements; Tetrad effect; Y/Ho ratio; Water–rock interaction; Groundwater; U deposit

## 1. Introduction

For many years, rare earth element (REE) patterns have been widely applied to deduce various geochem-

* Corresponding author.
*E-mail address:* takahasi@geol.sci.hiroshima-u.ac.jp (Y. Takahashi).
[1] Present address: Nagoya University Museum, Nagoya University, Nagoya 464-8601, Japan.

0009-2541/02/$ - see front matter 
PII: S0009-2541(01)00388-6

ical processes in geological materials (e.g., Henderson, 1984; Taylor and McLennan, 1988). For example, the overall trend in a REE pattern, which is mainly regulated by ionic radii, shows the source of the sample and the fractionation processes it has inherited. Cerium and Eu anomalies can reflect redox conditions when the sample was formed. In addition, the tetrad effect, another feature sometimes observed in REE patterns, is also a promising tool to deduce geochemical information from natural samples (e.g., Masuda and Ikeuchi, 1979; Kawabe et al., 1991; Bau, 1996). The tetrad effect is observed as concave curves consisting of La–Ce–Pr–Nd, Pm–Sm–Eu–Gd, Gd–Tb–Dy–Ho, and Er–Tm–Yb–Lu in REE patterns, details of which will be described in the next section. In addition, non-chondritic Y/Ho ratios have often been observed for samples which showed tetrad effects (Kawabe et al., 1991; Zhang et al., 1994; Bau, 1996). The primary aim of this study is to evaluate the behavior of REE (including Y in this study) during water–rock interaction by examining their abundances in rocks and groundwaters in the Tono area, Gifu, Japan. In particular, the tetrad effects and non-chondritic Y/Ho ratios in these samples have been investigated systematically.

The Tono area including the Tono uranium deposit, central Japan, has a well-analyzed water–rock system that can help us to study REE behavior during water–rock interactions. Many studies have revealed that groundwater has played a role in transporting uranium from the granitic rocks to the overlying sedimentary rocks around the Tono uranium deposit (Katayama et al., 1974; Doi et al., 1975; Hanamuro et al., 1995). It is often observed that U and REE partition between rock and water similarly during water–rock interactions, especially when carbonate complexation is dominant as dissolved species in the aqueous phase (McLennan and Taylor, 1979; Hidaka et al., 1992). Carbonate concentration in the groundwater of the Tono area is fairly high (ca. $4 \times 10^{-4}$ M; Iwatsuki and Yoshida, 1999). Based on the speciation calculation assuming carbonate complexation, phosphate formation, and hydrolysis, rare earth elements are probably solved as dissolved carbonate complex in the groundwater as will be shown in Table 8. This suggests that carbonate complexation of REE has allowed them to be transported from the granitic rocks to the sedimentary rocks by the water–rock interaction in the Tono area.

In conducting such a study, the analysis of both groundwater and rock specimens is highly important to understand the water–rock interaction completely such as done by Bau et al. (1998) and Aubert et al. (2001). Not many previous studies, however, have dealt both with the rocks and with the (ground) waters involved in water–rock systems. Therefore, REE abundances in the groundwater studied in this work provide important information on the REE behavior in the water–rock system.

For the purpose of estimating the REE migration, we also applied various other methods in this study in addition to bulk analyses. In order to simulate the REE behavior during water–rock interaction between the granitic rocks and the groundwater, leaching experiments in the laboratory were conducted. Successful analyses of REE abundances and U-series disequilibrium in the U-mineralized zone by secondary ion mass spectrometry (SIMS) have also been reported. This helped us to discuss the role of the groundwater in the addition of REE and U to the sedimentary rocks.

These results and bulk analyses enabled us to estimate REE migration in the Tono area mainly based on the tetrad effect and non-chondritic Y/Ho ratios. This in turn suggests that the degree of the tetrad effect observed in REE patterns and the variations of Y/Ho ratios are promising tools to deduce REE behavior during water–rock interactions.

## 2. Tetrad effect in REE pattern and non-chondritic Y/Ho ratio

The lanthanide tetrad effect was first discovered in a system for the liquid–liquid extraction of lanthanides (Peppard et al., 1969). The effect causes four separate curves, consisting of La–Ce–Pr–Nd, Pm–Sm–Eu–Gd, Gd–Tb–Dy–Ho, and Er–Tm–Yb–Lu, on logarithmic plots of the distribution coefficients against the order of the atomic numbers of the lanthanides. Similar effects in the REE patterns of natural samples were first reported by Masuda and Ikeuchi (1979). Although the question has sometimes been raised as to whether the tetrad effect can induce such REE fractionation in natural systems (e.g., McLennan, 1994), the existence of the fractionation has been confirmed by theoretical and experimental investigations (Kagi et al., 1993;

Bau, 1996; Bau et al., 1998; Irber, 1999; Kawabe, 1992, 1999; Kawabe et al., 1999a and the papers referred to therein; Kawabe et al., 1999b). In many cases, it has been shown that the W-type tetrad effect, the downward concave curve in a REE pattern, occurs in seawater and groundwater (e.g., Masuda and Ikeuchi, 1979; Masuda et al., 1987). In contrast, the M-type tetrad effect, upward concave curve, was observed for the counterpart solid material that reacted with these fluids. The direction of the tetrad effect (W- or M-type) can be explained by the difference in Gibbs free energies of REE species in both phases in the partitioning (e.g., Kawabe et al., 1999a). Examples of W- and M-type tetrad effects are shown in Fig. 1. However, there have been few examples showing the simultaneous appearance of conjugate W- and M-type tetrad effects in water and rock samples in a closed system. In this paper, an example of conjugate W- and M-type tetrad effects occurring simultaneously in such geological samples is presented. These data could be useful to estimate the behavior of REE during water–rock interactions in the Tono area.

In addition, the abundance ratio of Y and Ho, which shows similar geochemical behavior due to their similar ionic radii and same valence, was also investigated in this study. It has been reported that Y/Ho ratios would be discrepant from the chondritic value (=28.1, weight ratio calculated from Anders and Grevesse, 1989) for samples showing a tetrad effect (Kawabe et al., 1991; Zhang et al., 1994; Bau, 1996). Therefore, Y/Ho ratios have also been determined to investigate the REE behavior in water–rock interactions.

Based on the tetrad effects and non-chondritic Y/Ho ratios observed in the samples from the Tono area, the behavior of REE at the site, especially the processes involved in their transportation from the granitic rocks to the sedimentary rocks, could be constrained.

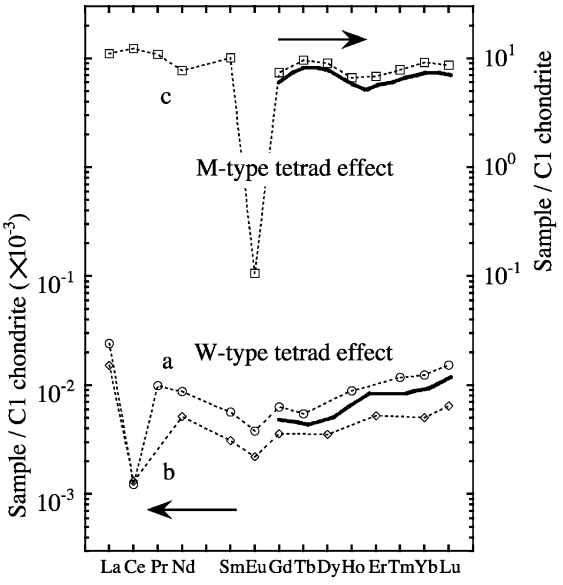


Fig. 1. Typical examples of W- and M-type tetrad effects observed in REE patterns of seawater and evolved granite. Seawater values were from (a) De Baar et al. (1985) and (b) Piepgras and Jacobsen (1992). Kawabe et al. (1998) showed that W-type tetrad effect appears in the REE patterns of seawater. REE values for the evolved granite were from (c) Irber (1999). The M-type tetrad effect in the evolved granite is considered to have formed by chemical complexation in an aqueous-like fluid system during the final stages of granite crystallization.

## 3. Geological background and previous studies for U-mineralization

Details of the geology in the Tono area were given by Ishihara and Suzuki (1969), Yamamoto et al. (1974), and Katayama and Kamiya (1977). The Tono uranium deposit lies within the Tertiary sedimentary rocks, Tono area, central Japan. The Tertiary sedimentary rocks are composed of the Mizunami Group (15–20 Ma) and the Seto Group (0.7–5 Ma), which unconformably overlies the basement (the Late Cretaceous Toki granite). The Tertiary sedimentary rocks are mainly composed of conglomerate (mainly granitic), tuffaceous rock with clastic minerals and lignite, arkose sandstone, and mudstone. The U-enrichment is found in a lower part of the Tertiary sedimentary rocks, which is a fluvial or lacustrine, lignite-bearing formation just above the unconformity between the granitic basement and the sedimentary rocks. Based on the fission-track method, the main U-mineralization is thought to have formed about 10 Ma (Ochiai et al., 1989).

The U-mineralization process has been described from the viewpoint of geology, mineralogy, and groundwater geochemistry (e.g., Katayama et al., 1974; Doi et al., 1975; Hanamuro et al., 1995). Hexavalent U leached from the granitic rocks was transported to the Tertiary sedimentary rocks, which

are reducing owing to the presence of organic matter. Since the solubility of U(IV) is extremely low, U(IV) generated by reduction was removed from groundwater and precipitated within the sedimentary rocks (Langmuir, 1978). The fact that $^{14}C$ ages of the groundwater near the U deposit (13,000–15,000 years) are distinct from those of groundwater of modern meteoric origin in the upper part of the sedimentary rocks (Seto groups) also supports the circulation of groundwater from the granite to the sedimentary rocks (Mizutani et al., 1992). Enrichment of U was found (1) in the cleavage of biotite flakes, (2) along the microfractures in detrital quartz grains, (3) at the margins of pyrite grains, and (4) as sorbed species onto clay minerals. In most cases, the major U mineral in the U-enriched zone is reported to be coffinite (Yamamoto et al., 1974; Yoshida, 1994).

## 4. Samples

### 4.1. Granite

Samples of the Toki granitic rocks were obtained from drilling cores and surface outcrops from the Tono area including the Tono uranium mine as shown in Fig. 2. Samples of drill core are mainly from two cores (KNA-6 and BH-1) drilled from a gallery constructed

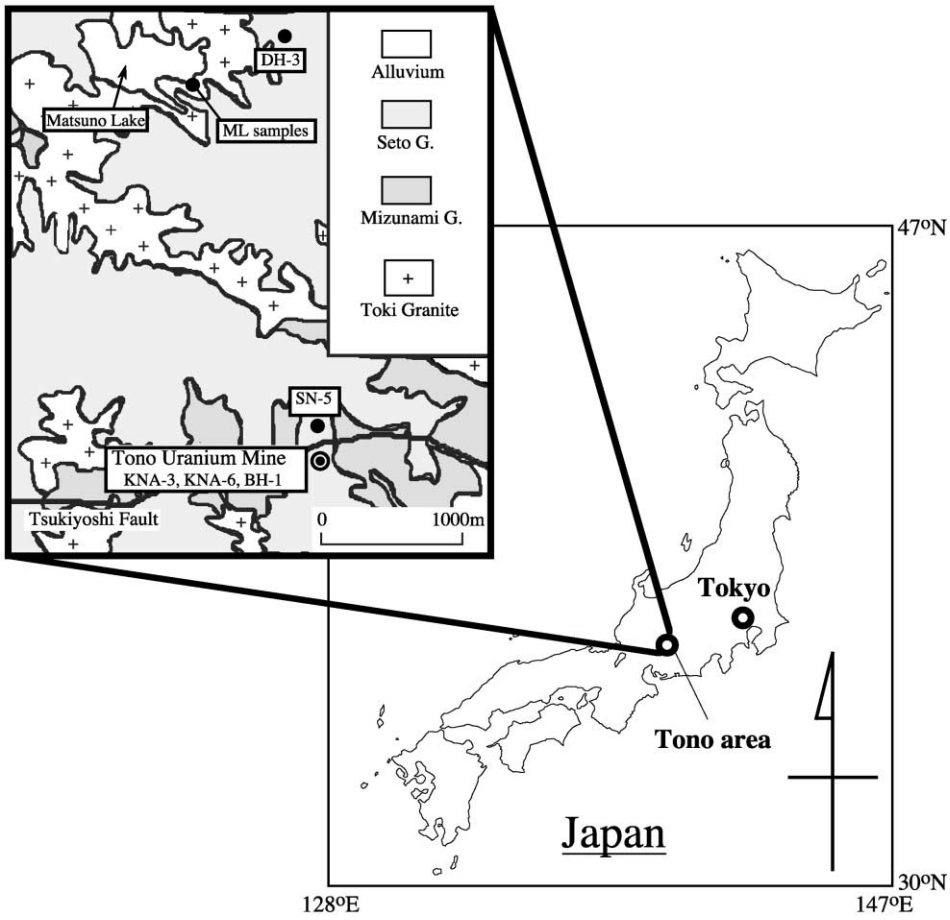


Fig. 2. Geological map of the Tono area modified from Iwatsuki and Yoshida (1999). Locations of drilling cores, Matsuno Lake, and a sampling point of weathered granite samples from outcrop (ML samples) were shown in the left figure. Details of Seto G. (Seto Group) and Mizunami G. (Mizunami Group) were described in Section 3.

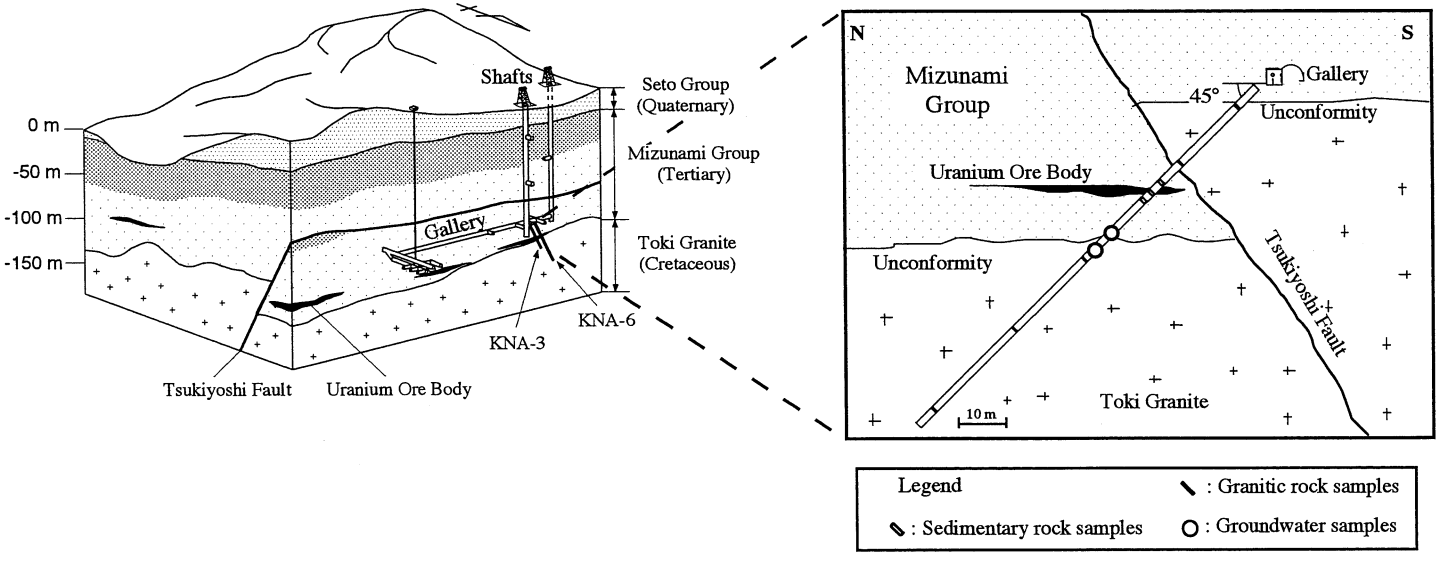


Fig. 3. Schematic view of KNA-3 and KNA-6 drilling sites. The KNA-3 and KNA-6 cores run parallel to each other.

at 130 m below ground surface. Another sample was obtained from boreholes drilled from ground level (SN-5). A schematic view of KNA-6 core, which was also similar to KNA-3 core, and a geological overview of the Tono uranium mine are shown in Fig. 3. The cores were drilled through the Tsukiyoshi Fault and sedimentary rocks, and terminated in the basement granite. Granite samples were collected from 6.7, 24.8, 54.9, 76.9, and 101 m in the KNA-6 core. The BH-1 core was also drilled from the gallery and core samples from 9.7, 24, and 49.3 m depths were analyzed in this study. Core samples from 149.8 m depth in the SN-5 core and from 504 m depth in the DH-3 core were also studied. Eight samples were taken from surface outcrops of the Toki granite near the Matsuno Lake (ML-1, ML-2, ML-3a, ML-3b, ML-5, ML-7, ML-8, ML-9).

The degrees of weathering of these granitic rocks were placed into categories from A to E according to the classification by Toyoda et al. (1999) as noted in Table 1. The five classifications are A (fresh), B (slightly weathered), C (weakly weathered), D (strongly weathered), and E (disaggregated), the definitions of which are shown in the footnote of Table 1.

### 4.2. Sedimentary rocks

Samples of the sedimentary rocks were obtained from the KNA-3 core, which was drilled parallel to KNA-6. The samples from 31.7 (divided into coarse and fine grained parts), 35.4 and 38.0 m were analyzed (Fig. 3). These points correspond to 151, 153, and 155 m depths from the ground surface, respectively. The U ore body lies around the point at 38.0 m in the KNA-3 section (Yoshida et al., 1994). For the SIMS analysis, the sample at 31.7 m depth (coarse grain part) was employed. A brief description of each sample was made in Table 2.

### 4.3. Groundwater

The sampling of groundwater was carried out with double-packer systems installed in boreholes KNA-6

Table 1
Major element compositions (wt.%) of granite rocks and the degree of weathering to which each sample has been subjected. The chemical index of alteration (CIA) calculated from major element composition and porosity ($n_p$) determined in this study are also listed

| Sample | $SiO_2$ | $TiO_2$ | $Al_2O_3$ | $Fe_2O_3$[a] | MnO | MgO | CaO | $Na_2O$ | $K_2O$ | $P_2O_5$ | Weathering[b] | CIA | $n_p$ |
|---|---|---|---|---|---|---|---|---|---|---|---|---|---|
| *From drilling core* | | | | | | | | | | | | | |
| KNA-6 6.7 m | 75.84 | 0.18 | 13.51 | 2.07 | 0.05 | 0.32 | 0.91 | 3.05 | 4.91 | 0.01 | D (strongly) | 54.8 | 31 |
| KNA-6 24.8 m | 76.23 | 0.14 | 13.71 | 1.59 | 0.02 | 0.19 | 0.40 | 3.60 | 5.46 | 0.03 | C (weakly) | 52.9 | 11 |
| KNA-6 54.9 m | 77.33 | 0.20 | 13.08 | 2.07 | 0.04 | 0.33 | 1.08 | 3.22 | 4.22 | 0.03 | D (strongly) | 54.7 | 29 |
| KNA-6 76.9 m | 74.11 | 0.28 | 13.82 | 2.67 | 0.06 | 0.40 | 1.31 | 3.39 | 4.17 | 0.07 | C (weakly) | 55.0 | 14 |
| KNA-6 101.0 m | 74.42 | 0.13 | 14.46 | 1.50 | 0.05 | 0.27 | 1.84 | 4.00 | 4.58 | 0.04 | B (slightly) | 52.3 | 4.4 |
| BH-1 9.7 m | 74.20 | 0.16 | 13.08 | 1.84 | 0.04 | 0.27 | 0.97 | 3.38 | 4.90 | 0.04 | C (weakly) | 52.7 | 12 |
| BH-1 24 m | 75.51 | 0.16 | 12.83 | 1.68 | 0.04 | 0.27 | 0.87 | 3.16 | 5.00 | 0.04 | C (weakly) | 53.0 | 13 |
| BH-1 49.3 m | 74.12 | 0.15 | 13.74 | 1.63 | 0.05 | 0.28 | 1.35 | 3.78 | 4.46 | 0.04 | C (weakly) | 52.8 | 7.2 |
| SN-5 149.8 m | 73.37 | 0.19 | 13.64 | 1.94 | 0.06 | 0.33 | 1.34 | 3.68 | 4.29 | 0.05 | A (fresh) | 53.4 | 6.2 |
| DH-3 504 m | 74.12 | 0.15 | 13.74 | 1.63 | 0.05 | 0.28 | 1.35 | 3.78 | 4.46 | 0.04 | A (fresh) | 52.8 | 3.0 |
| *From surface outcrop* | | | | | | | | | | | | | |
| ML-1 | 77.07 | 0.04 | 13.80 | 0.91 | 0.04 | 0.06 | 0.30 | 1.97 | 4.80 | 0.01 | E (disaggregated) | 61.3 | 52 |
| ML-2 | 75.64 | 0.08 | 14.53 | 1.36 | 0.03 | 0.09 | 0.39 | 2.13 | 4.83 | 0.01 | E (disaggregated) | 61.5 | 27 |
| ML-3R | 75.03 | 0.05 | 13.79 | 1.02 | 0.03 | 0.06 | 0.73 | 3.52 | 4.93 | 0.01 | C (weakly) | 53.9 | 9.1 |
| ML-3W | 74.20 | 0.08 | 13.72 | 1.35 | 0.04 | 0.10 | 0.65 | 3.43 | 5.23 | 0.01 | B (slightly) | 53.6 | 10 |
| ML-5 | 77.82 | 0.10 | 12.64 | 1.55 | 0.04 | 0.10 | 0.40 | 2.15 | 4.99 | 0.02 | E (disaggregated) | 57.6 | – |
| ML-7 | 74.05 | 0.06 | 14.67 | 1.22 | 0.03 | 0.06 | 0.64 | 3.70 | 5.32 | 0.01 | D (strongly) | 54.1 | 9.2 |
| ML-8 | 75.87 | 0.04 | 14.03 | 0.73 | 0.02 | 0.05 | 0.27 | 2.06 | 6.06 | 0.01 | E (disaggregated) | 57.9 | 29 |
| ML-9 | 77.13 | 0.05 | 13.49 | 0.84 | 0.02 | 0.07 | 0.28 | 1.71 | 5.21 | 0.01 | E (disaggregated) | 60.8 | 32 |

[a] Total iron as $Fe_2O_3$.

[b] The definition of A to E is as follows. A (fresh): Very hard. Difficult to crush by hammer. B (slightly weathered): Hard. Metallic sound on hitting with hammer. C (weakly weathered): Moderately hard. Crushed easily by hammer. D (strongly weathered): Friable. Crushed to fine grains by hammer. E (disaggregated): Totally crumbled. Clays.

Table 2
Major element compositions (wt.%) and some descriptions of the sedimentary rocks obtained from KNA-3

| Sample | $SiO_2$ | $TiO_2$ | $Al_2O_3$ | $Fe_2O_3$[a] | MnO | MgO | CaO | $Na_2O$ | $K_2O$ | $P_2O_5$ | Description |
|---|---|---|---|---|---|---|---|---|---|---|---|
| 31.7 m (fine part) | 36.16 | 0.39 | 12.70 | 7.34 | 0.36 | 3.01 | 12.68 | 1.08 | 0.40 | 0.39 | calcite-bearing mudstone |
| 31.7 m (coarse part) | 64.84 | 0.59 | 15.47 | 5.81 | 0.09 | 1.81 | 4.07 | 2.57 | 2.91 | 0.43 | arkose |
| 35.4 m | 67.16 | 0.49 | 14.70 | 1.96 | 0.04 | 0.64 | 2.53 | 2.84 | 3.53 | 0.61 | arkose |
| 38.0 m | 55.84 | 1.33 | 21.23 | 5.18 | 0.14 | 1.78 | 7.47 | 2.62 | 0.99 | 0.88 | mudstone |

[a] Total iron as $Fe_2O_3$.

and KNA-2 that run parallel to KNA-6. Two groundwater samples were obtained from the KNA-6 borehole: one is from the unconformity between the granitic rocks and the sedimentary rocks, which is just below the U-mineralized zone, and the other is from the granitic rocks just below the unconformity, as shown in Fig. 3. Another groundwater sample was also obtained from the unconformity in the KNA-2 borehole. In-situ values of Eh, pH, electronic conductivity (EC), and temperature for the groundwater have been measured with a remote monitoring system (Yoshida et al., 1994; Iwatsuki and Yoshida, 1999) (Table 3). Major element compositions were also reported in Iwatsuki and Yoshida (1999) and U concentration was determined in this study (Table 3).

Two methods were used to collect waters from the KNA-6 borehole. In one method, a small amount of high-purity 60% $HNO_3$ was added to the sample after filtering the groundwater with a 0.45 μm membrane filter until the $HNO_3$ content became 2%. The REE included in this sample can be regarded as the dissolved fraction in the groundwater including colloidal REE that can pass through 0.45 μm membrane filter. The fraction is designated as $REE_{dis}$, though we should note that the fraction may also include colloidal REE that can pass through 0.45 μm membrane filter. In the other method, the unfiltered sample was mixed with the same amount of 60% $HNO_3$. After two weeks, the sample was filtered (0.45 μm), and is referred to as ($REE_{sorb} + REE_{dis}$). The latter sample, acidified before filtration, includes both the initially dissolved species ($REE_{dis}$) and the exchangeable REE initially sorbed on particulate matter that can be desorbed by 2% $HNO_3$ ($REE_{sorb}$). As reference materials, three surface waters were also collected. One is from a small stream and the others are from ponds (Higashibora Pond and Shizubora Pond) in the Tono area. These samples were filtered and acidified with $HNO_3$. The pH, EC, Eh, and temperature are also listed in Table 3.

## 5. Analytical procedures

### *5.1. Major element, REE, and U abundances for rock samples*

Major element compositions were analyzed by X-ray fluorescence spectrometry (Philips PW1404), by employing fused glasses made from a mixture of

Table 3
Physico-chemical properties of groundwater and surface water examined in this study with U concentration

| | KNA-6 borehole | | KNA-2 borehole | A stream near the Tono mine | Higashibora pond | Shizubora pond |
|---|---|---|---|---|---|---|
| | Unconformity | Granite | Unconformity | | | |
| pH | 9.41 | 8.49 | 9.09 | 9.52 | 8.80 | 9.08 |
| EC (μS/cm) | 189 | 174 | 182 | 39.4 | 30.1 | 46.2 |
| Eh (mV) | −300 | 0 | −107 | 218 | 173 | 163 |
| Temperature | 18.1 | 15.9 | 17.6 | 9.0 | 11.7 | 10.4 |
| Dissolved Oxygen (mg/l) | 0 | 0 | 0 | – | – | – |
| Inorganic carbon (ppm) | 23.4 | 21.6 | – | – | – | – |
| U (ppt) | 1.8 | 31 | 9.4 | 19 | 24 | 85 |

sample and $Li_2B_4O_7$. Calibration was done by using standard rocks prepared by the Geological Survey of Japan (Imai et al., 1995).

REE abundances were determined by inductively coupled plasma-mass spectrometry (ICP-MS; VG PQ-3). About 0.1 g of weighed sample for each granitic rock or sedimentary rock was decomposed by heating (ca. 180 °C) for more than three days in a mixture of $HClO_4$ and HF in a teflon vessel with a screw cap. REE in the decomposed solution were separated by a cation-exchange method employing a column with AG50W-X8 resin. The REE fraction was finally redissolved with 2% $HNO_3$ for injection into the ICP-MS. The REE abundances were determined using In and Bi as internal standards for ICP-MS analysis. The REE isotopes monitored with ICP-MS were $^{139}La$, $^{140}Ce$, $^{141}Pr$, $^{146}Nd$, $^{149}Sm$, $^{151}Eu$, $^{157}Gd$, $^{159}Tb$, $^{163}Dy$, $^{165}Ho$, $^{166}Er$, $^{169}Tm$, $^{172}Yb$, and $^{175}Lu$. Calibration curves were made by using 10 ppt, 50 ppt, 100 ppt, 500 ppt, 1 ppb, 5 ppb, and 10 ppb REE solutions prepared from the REE standard solution (10 ppm) obtained from SPEX CertiPrep. Each sample was diluted by a factor appropriate to reduce all REE concentrations of the analyzed solution to lie within the region of the standard solutions (i.e., from 10 ppt to 10 ppb). The number of samples measured in one analysis was restricted to be lower than 6 so as to measure all samples and standards under stable ICP-MS conditions. Measured $REE\text{-}O^+/REE^+$ ratios were lower than 1.5% in our analyses. Oxide corrections were made for $^{151}Eu$ and $^{157}Gd$ that were interfered with by the $^{135}BaO$ peak and the $^{140}CeOH$ and $^{141}PrO$ peaks, respectively (Shinotsuka et al., 1996). For the correction, single-element solutions of Ba, Ce, and Pr were measured immediately after the samples and standards to obtain the ratios of BaO/Ba (normally less than 0.001 in our analyses), CeOH/Ce ($<0.001$), and PrO/Pr ($<0.015$) for every analysis. These ratios were employed to correct the intensities of $^{151}Eu$ and $^{157}Gd$. The precision and difference from the recommended values (Imai et al., 1995) were obtained by repeated analyses, including decomposition processes, of the standard rocks JB-1a and JG-1a received from the Geological Survey of Japan. The precision for each REE was better than 5% except for Tm (6%). The REE abundances for JB-1a (basalt) agreed with the recommended values to within 5%, except for Y, Ho and Lu (ca. 10–15% for these elements). Values for JG-1a (granodiorite) were better than 8% except for Y, Pr, Tb, and Lu (ca. 10% for these elements). Such differences for Y, Pr, Tb, and Ho can be expected, since these elements are monoisotopic elements and precise isotope dilution analyses are impossible for them as noted by Shinotsuka et al. (1996).

For U determination, the 0.5 M HCl solution prepared for the REE analysis was dried and redissolved by 2% $HNO_3$. The U content in the solution was determined by ICP-MS without any separation and Bi was employed as an internal standard.

### *5.2. REE and U in water samples and leaching experiments*

The concentrations of some elements among the REE in groundwater are generally even lower than ppt level. Hence, the analytical method for REE in groundwater involved preconcentration by cation-exchange with an AG50W-X8 column (diameter: 8 mm; resin volume: 2.5 $cm^3$ in 0.5 M HCl solution), following the method developed by Stetzenbach et al. (1994). A similar method was also employed by Johannesson and Hendry (1999) and Johannesson et al. (1996). After the column was eluted with 6 M HCl solution, 2% $HNO_3$ was injected to equilibrate the resin with the solution. After introducing about 500 $dm^3$ of water sample (acidified to 2% $HNO_3$) into the column, major elements were eluted by 2 M HCl solution before collecting the REE bearing fraction. The REE was eluted by 37 $dm^3$ of 6 M HCl solution. The eluted solution containing REE was evaporated to dryness and redissolved by ca. 5 ml of 2% $HNO_3$ solution for the ICP-MS analysis. By this method, the preconcentration factor was about 100. The analytical procedure by ICP-MS was similar to that employed for rock samples, except that an optional backing rotary pump (s-option pump) was employed which was connected behind the rotary pump in the expansion region of the ICP-MS to achieve better vacuum in the expansion region. The use of the s-option pump increased the sensitivity of the ICP-MS up to three times. The concentrations of standards used for the calibrations were 1 ppt, 5 ppt, 10 ppt, 50 ppt, 100 ppt, 500 ppt, and 1 ppb. All samples analyzed here were included in the calibrated region with these standards. Even in the sample having the lowest REE concentrations (filtered sample from granite), we could

obtain more than 200 cps for all REE in our analyses. The $^{135}$BaO signal among the total counts at mass number 151 (Eu) is corrected in a similar way as for the rock analyses, though the highest percentage of $^{135}$BaO contribution reached 40% for this mass in the filtered groundwater sample from granite. The interferences of CeOH and PrO were less than 10% for the $^{157}$Gd peak.

The preconcentration factor could not be increased to more than 100, since higher preconcentration factor led to the instability of the ICP-MS during the measurement as suggested by Stetzenbach et al. (1994). Such instability was presumably caused by the preconcentration of solutes, other than REE, that could not be removed by the ion-exchange method. Analyses of a standard REE solution by an identical method determined that the recoveries of REE with this method were better than 97% for all REE elements. Background REE abundances given by the whole analytical procedure were measured three times (Table 5). The REE abundances in surface waters were determined by the similar method applied to groundwater.

Before measuring U abundances in water samples, the water was preconcentrated to about five times by direct evaporation. Bismuth was employed as an internal standard for the U measurement by ICP-MS. Uranium concentration was determined with the s-option pump on.

In order to simulate water–rock interactions in laboratory experiments, powdered sample of the granitic rock (10 g) recovered from KNA-6 at 54.9 m point was soaked in pure Milli-Q water (50 g) in a teflon vessel. Two systems were examined as follows:

System A—NaHCO3 was not added; final pH: 7.32.
System B—NaHCO3 was added (0.38 mM); final pH: 9.20.

The concentration of $NaHCO_3$ for system B (0.38 mM) was chosen to give a similar concentration of total carbonate as that in groundwater from granite in the Tono area (Iwatsuki and Yoshida, 1999). The samples for the system A was soaked in water for 212 days. The sample for the system B was shaken for 2 weeks at ambient room temperature. The aqueous phase was filtered with a 0.45 μm membrane filter. The REE abundance leached to the water was determined using an identical method to that used for the groundwater analyses.

### *5.3. REE abundances and disequilibrium of U-series in U-mineralization zone by SIMS*

The REE abundances of U-mineralization zone in the sedimentary rocks were measured by SIMS (SHRIMP II). Uraninite ($UO_2$) from Mistamisk, Canada (Kish and Cuney, 1981) was used as a standard sample. The piece of the Mistamisk uraninite was large enough (ca. 1 cm × 1 cm × 0.5 cm) to enable small fragments (ca. 5 mg) to be picked out. Each fragment was decomposed to measure the REE abundances by ICP-MS. The REE patterns of seven different pieces of the standard sample are shown in Fig. 4. The Mistamisk sample showed homogeneous distributions of REE over the grain except for Ce, Pr, and Nd. This meets the requirement of a standard sample for SIMS analysis, that is, to be homogeneous.

The instrumental conditions employed for REE analysis by SIMS were similar to those of Sano et al. (1999, 2000). The intensities of isotopes of REE

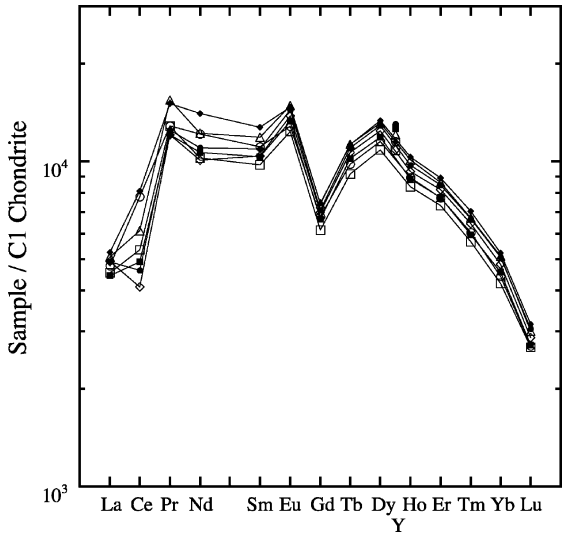


Fig. 4. Chondrite-normalized REE patterns of Mistamisk uraninite. Seven patterns are given from independent results for seven pieces picked out from one grain of Mistamisk uraninite. For the normalization, REE abundances in C1 chondrite (Anders and Grevesse, 1989) were employed.

Table 4
REE and U abundances (ppm) and various indices in REE pattern of the Toki granites. Explanation of $(Ln)_{CN}/(Ln^*)_{CN}$ is describe in Section 6.1

| | KNA-6 | | | | | BH-1 | | | SN-5 | ML1 | ML2 | ML3R | ML3W | ML5 | ML7 |
|---|---|---|---|---|---|---|---|---|---|---|---|---|---|---|---|
| | 6.7 m | 24.8 m | 54.9 m | 76.9 m | 101 m | 9.7 m | 24 m | 49.3 m | 149.8 m | | | | | | |
| Y | 29.4 | 26.4 | 37.0 | 52.7 | 23.6 | 33.1 | 27.4 | 34.6 | 34.1 | 38.9 | 90.6 | 39.4 | 33.1 | 48.7 | 37.5 |
| La | 22.2 | 15.4 | 25.6 | 33.0 | 17.9 | 19.4 | 17.4 | 23.8 | 19.4 | 7.5 | 45.1 | 11.4 | 16.0 | 16.1 | 12.6 |
| Ce | 40.3 | 34.4 | 52.7 | 65.4 | 35.9 | 38.9 | 36.5 | 46.4 | 40.0 | 58.5 | 66.0 | 29.5 | 36.1 | 34.4 | 25.5 |
| Pr | 5.22 | 3.56 | 5.90 | 7.39 | 3.99 | 4.65 | 4.02 | 5.06 | 4.58 | 2.17 | 12.2 | 3.07 | 4.24 | 4.36 | 3.37 |
| Nd | 19.0 | 12.8 | 20.8 | 26.7 | 14.2 | 16.6 | 14.7 | 18.3 | 16.9 | 8.19 | 48.9 | 12.5 | 15.9 | 16.7 | 12.8 |
| Sm | 4.16 | 2.91 | 4.71 | 6.27 | 3.20 | 4.16 | 3.51 | 4.29 | 4.15 | 2.70 | 12.4 | 3.86 | 4.49 | 5.04 | 3.78 |
| Eu | 0.575 | 0.458 | 0.716 | 0.611 | 0.571 | 0.549 | 0.439 | 0.606 | 0.401 | 0.129 | 0.521 | 0.195 | 0.226 | 0.217 | 0.199 |
| Gd | 3.77 | 3.03 | 4.44 | 6.48 | 3.23 | 4.50 | 3.80 | 4.45 | 4.54 | 3.99 | 14.0 | 4.59 | 4.85 | 6.11 | 4.42 |
| Tb | 0.818 | 0.620 | 0.946 | 1.21 | 0.598 | 0.848 | 0.688 | 0.842 | 0.859 | 0.903 | 2.42 | 0.852 | 0.982 | 1.24 | 0.922 |
| Dy | 5.05 | 4.33 | 6.02 | 8.40 | 4.07 | 5.50 | 4.38 | 5.57 | 5.61 | 6.54 | 15.6 | 5.68 | 6.17 | 8.27 | 6.27 |
| Ho | 1.07 | 0.951 | 1.31 | 1.80 | 0.859 | 1.24 | 0.98 | 1.22 | 1.24 | 1.48 | 3.17 | 1.19 | 1.32 | 1.80 | 1.40 |
| Er | 3.48 | 3.21 | 4.41 | 5.91 | 2.66 | 3.84 | 3.01 | 3.92 | 3.88 | 4.83 | 9.17 | 3.68 | 4.01 | 5.58 | 4.35 |
| Tm | 0.534 | 0.518 | 0.718 | 0.993 | 0.422 | 0.625 | 0.504 | 0.646 | 0.655 | 0.772 | 1.35 | 0.558 | 0.628 | 0.883 | 0.693 |
| Yb | 3.78 | 3.82 | 4.96 | 6.90 | 2.92 | 4.41 | 3.27 | 4.61 | 4.43 | 5.45 | 8.18 | 3.78 | 4.24 | 5.99 | 4.71 |
| Lu | 0.553 | 0.573 | 0.748 | 1.02 | 0.431 | 0.649 | 0.521 | 0.669 | 0.693 | 0.744 | 0.880 | 0.568 | 0.628 | 0.880 | 0.698 |
| U | 7.06 | 6.17 | 5.59 | 87.0 | 5.60 | 5.05 | 4.10 | 3.85 | 4.88 | – | – | – | – | – | – |
| Y/Ho | 27.4 | 27.8 | 28.3 | 28.6 | 29.0 | 26.6 | 27.9 | 28.3 | 27.5 | 26.2 | 28.5 | 33.1 | 25.1 | 27.0 | 26.7 |
| $(Pr)_{CN}/(Pr^*)_{CN}$ | 1.06 | 1.06 | 1.08 | 1.04 | 1.06 | 1.08 | 1.05 | 1.03 | 1.06 | 1.11 | 1.05 | 1.03 | 1.08 | 1.08 | 1.08 |
| $(Tb)_{CN}/(Tb^*)_{CN}$ | 1.17 | 1.07 | 1.14 | 1.12 | 1.02 | 1.03 | 1.01 | 1.03 | 1.04 | 1.12 | 1.01 | 1.03 | 1.11 | 1.08 | 1.09 |
| $(Dy)_{CN}/(Dy^*)_{CN}$ | 1.08 | 1.08 | 1.07 | 1.06 | 1.06 | 1.01 | 0.994 | 1.03 | 1.02 | 1.11 | 1.04 | 1.06 | 1.06 | 1.07 | 1.06 |
| $(Tm)_{CN}/(Tm^*)_{CN}$ | 1.00 | 1.01 | 1.03 | 0.97 | 1.02 | 1.03 | 1.06 | 1.04 | 1.05 | 1.05 | 1.13 | 0.993 | 1.02 | 1.03 | 1.03 |
| $(Yb)_{CN}/(Yb^*)_{CN}$ | 1.03 | 1.05 | 1.03 | 1.01 | 1.03 | 1.05 | 0.979 | 1.07 | 1.01 | 1.10 | 1.19 | 1.00 | 1.02 | 1.03 | 1.03 |

and U were analyzed in high-resolution mode ($M/dM > 8500$; $M$: mass number; dM: peak width at 1% peak height). With the method, it was possible to separate isobaric interference of LREE oxide with HREE ion peak such as $^{141}Pr^{16}O^+$ with $^{157}Gd^+$. The abundances of REE in the sample were obtained by comparing the ratio of ($REE^+/U^+$) in the sample with the ratio of the Mistamisk uraninite. Uranium concentration at the spot for SIMS analysis, which was needed to obtain absolute concentration of REE, was determined by EPMA. The peak of $^{235}U$ was employed to monitor U concentration, since the intensity of the $^{238}U$ peak was too large to be counted by the electron multiplier in SIMS analysis in the same scan as the $REE^+$ ions.

Disequilibrium of U-series nuclides was also examined by SIMS. The intensities of the $^{234}U^+$ and $^{235}U^+$ peaks were measured; $^{234}U^+$ gave ca. 15 cps for the U mineral examined in this study. In the analysis, the $^{238}U$ peak was not measured due to its extremely large intensity when monitored simultaneously with $^{234}U$. The intensity of the $^{238}U$ peak was estimated from the intensity of the $^{235}U$ peak by assuming a ratio of $^{235}U$:$^{238}U = 1$:137.8. The ratios of the observed intensities were transformed to the activity ratios:

$$(^{234}U)_{ac}/(^{238}U)_{ac} = f\lambda_{234}/\lambda_{238}(^{234}U^+)/[(^{235}U^+)137.8], \quad (1)$$

where subscript ac denotes the activity; $\lambda$, the decay constant. The mass discrimination of $^{234}U$ and $^{235}U$ is estimated to be lower than 0.18%, estimated from the value for $^{207}Pb$ to $^{206}Pb$ (0.18%) obtained for the same instrument (Sano et al., 2000). Since $(^{234}U)_{ac}/(^{238}U)_{ac}$ for our sample varied by more than 10%, as shown later, we regarded $f$ as unity in this work. In order to check the validity of the analysis, $(^{234}U)_{ac}/(^{238}U)_{ac}$ was estimated by Eq. (1) for uraninite sample obtained from Retail pitchblende (France) having an age of 425 Ma (Holliger, 1988), which is enough for the U-series to reach their equilibrium. The $(^{234}U)_{ac}/(^{238}U)_{ac}$ for the Retail pitchblende by the present method was $1.01 \pm 0.02$. This also shows that we can analyze the variation of $(^{234}U)_{ac}/(^{238}U)_{ac}$ in the U-mineralization zone by SIMS.

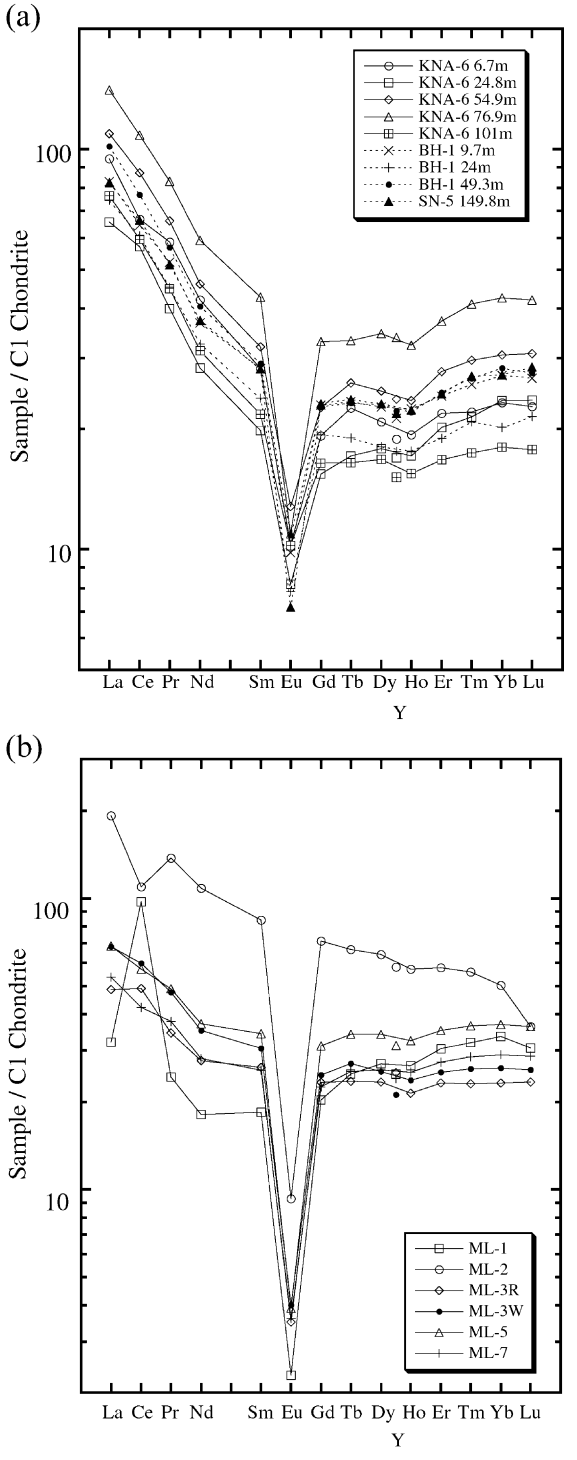


Fig. 5. Chondrite-normalized REE patterns of the Toki granitic rocks obtained from (a) drilling cores and (b) surface outcrop.

## 6. Results

### 6.1. Granite

Major elements compositions in the Toki granitic rocks are listed in Table 1 together with the classification of degrees of weathering (A to E). As an index for the degree of weathering to which granitic rock samples have been subjected, CIA values were calculated from the molar ratios of major elements (Table 1), following Nesbitt and Young (1982),

$$\mathrm{CIA} = 100 \times \mathrm{Al_2O_3}/(\mathrm{Na_2O} + \mathrm{K_2O} + \mathrm{CaO} + \mathrm{Al_2O_3}). \quad (2)$$

Generally, a CIA value has been reported to be 45–55 for fresh granite, 50 for unaltered feldspar, 75–85 for montmorillonite, and 100 for kaolinite (Nesbitt and Young, 1982). The CIA values of weathered granite or granodiorite are variable, in the range of 50–70 (e.g., Condie et al., 1995). The CIA values for the Toki granitic rocks from surface outcrops near Matsuno Lake ranged from 52 to 61. The CIA values of the Toki granitic rocks from drill cores were in a narrower range, from 49 to 53. This reveals that the granitic rocks from drill cores are less chemically weathered compared with the samples from the surface outcrops. However, some of the granitic rocks from drill cores were very friable, showing that they were physically weathered or tectonically fractured. As another index for the degree of weathering, porosity ($n_p$) was determined for the granitic rock specimens by Eq. (3):

$$n_p = \rho_{H_2O}(W_s - W_d)/(W_d/\rho_{SP}), \quad (3)$$

where $W_s$ is water-saturated and surface-dry weight; $W_d$, dry weight; $\rho_{SP}$, density of sample. The $n_p$ values determined for the granite samples were also listed in Table 1. The $n_p$ values correlated with the weathering classification of A–E. For strongly weathered samples, $n_p$ even reached around 30%; for weakly weathered samples, $n_p$ values were 10–15%; for slightly weathered and fresh granite, $n_p$ values were less than 8%.

Table 5
REE abundances (ppt) and various indices in the groundwater recovered from the Tono area. The sample of unconformity and granite was obtained from borehole KNA-3. The KNA-2 sample was recovered from the unconformity. The result of the blank analyses are also shown

| | Unconformity | | Granite | | KNA-2 | Blank[a] |
|---|---|---|---|---|---|---|
| | Filtered | Unfiltered | Filtered | Unfiltered | Filtered | ($n=3$) |
| Y | 12.8 | 17.3 | 7.7 | 9.2 | 15.6 | 0.028 ± 0.013 |
| La | 1.39 | 3.18 | 1.67 | 4.81 | 1.80 | 0.26 ± 0.09 |
| Ce | 2.64 | 6.06 | 2.29 | 8.36 | 3.97 | 0.39 ± 0.15 |
| Pr | 0.35 | 0.76 | 0.28 | 0.92 | 0.563 | 0.056 ± 0.029 |
| Nd | 1.87 | 3.47 | 1.19 | 3.69 | 2.68 | 0.14 ± 0.06 |
| Sm | 0.634 | 1.04 | 0.257 | 0.744 | 0.822 | 0.019 ± 0.0004 |
| Eu | 0.108 | 0.144 | 0.041 | 0.098 | 0.057 | 0.0011 ± 0.001 |
| Gd | 1.02 | 1.66 | 0.389 | 0.859 | 0.705 | 0.011 ± 0.001 |
| Tb | 0.178 | 0.267 | 0.054 | 0.139 | 0.110 | 0.0021 ± 0.0003 |
| Dy | 1.10 | 1.81 | 0.391 | 0.899 | 0.754 | 0.0072 ± 0.0006 |
| Ho | 0.282 | 0.413 | 0.109 | 0.213 | 0.196 | 0.00087 ± 0.00037 |
| Er | 0.801 | 1.15 | 0.352 | 0.633 | 0.723 | 0.0038 ± 0.0016 |
| Tm | 0.099 | 0.129 | 0.045 | 0.090 | 0.106 | 0.00042 ± 0.00014 |
| Yb | 0.461 | 0.634 | 0.278 | 0.490 | 0.613 | 0.0045 ± 0.0032 |
| Lu | 0.074 | 0.088 | 0.042 | 0.073 | 0.112 | 0.00063 ± 0.00027 |
| Y/Ho | 45.4 | 41.8 | 71.3 | 43.4 | 79.7 | |
| $(Pr)_{CN}/(Pr^*)_{CN}$ | 0.855 | 0.923 | 0.851 | 0.930 | 0.977 | |
| $(Tb)_{CN}/(Tb^*)_{CN}$ | 0.948 | 0.908 | 0.751 | 0.913 | 0.852 | |
| $(Dy)_{CN}/(Dy^*)_{CN}$ | 0.887 | 0.964 | 0.822 | 0.927 | 0.878 | |
| $(Tm)_{CN}/(Tm^*)_{CN}$ | 0.956 | 0.925 | 0.912 | 1.023 | 0.960 | |
| $(Yb)_{CN}/(Tb^*)_{CN}$ | 0.783 | 0.853 | 0.916 | 0.915 | 0.820 | |

[a] Errors shown in the blank are 1$\sigma$.

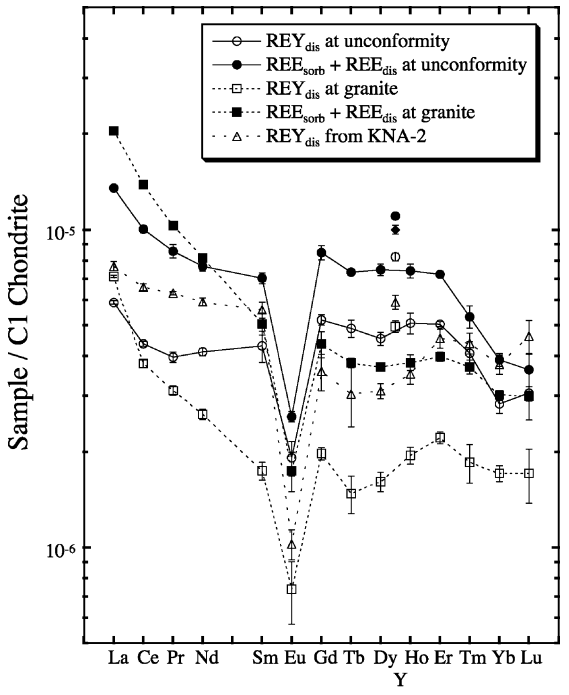


Fig. 6. Chondrite-normalized REE patterns of the groundwater recovered from the boreholes of KNA-6 and KNA-2. From the borehole of KNA-6, groundwater samples in the granite and at the unconformity were obtained. The $REE_{dis}$ denotes the REE species passed through 0.45 μm filter, while $REE_{sorb}$ shows the fraction of sorbed species that can be released by 2% nitric acid. The patterns of $REE_{dis}$ and ($REE_{dis}$ + $REE_{sorb}$) directly obtained by the experiments are shown.

This correlation implies that the porosity reflects the degree of weathering the sample has been subjected to.

The REE and U abundances for the Toki granite are shown in Table 4. Chondrite-normalized REE patterns of the Toki granitic rocks are shown in Fig. 5a and b. For the normalization, REE abundances in C1 chondrite (Anders and Grevesse, 1989) were employed. In some of these patterns, M-type tetrad effects are observed. Since the recovery of REE from their column separation was better than 97% for all REE, there is no possibility for the appearance of tetrad effect through the separation procedure for the REE analysis. The degree of the tetrad effect, for example for Dy, can be expressed as:

$$(\mathrm{Dy})_{\mathrm{CN}}/(\mathrm{Dy}^{*})_{\mathrm{CN}} = (\mathrm{Dy})_{\mathrm{CN}}/\left\{(\mathrm{Gd})_{\mathrm{CN}}^{1/3}(\mathrm{Ho})_{\mathrm{CN}}^{2/3}\right\}, \quad (4)$$

where subscript CN denotes the chondrite-normalized value (cf. Irber, 1999). In a similar way, corresponding values were also obtained for Pr, Tb, Tm, and Yb (Table 4), but not for Ce, Sm, and Eu due to a lack of Pm data and the anomalous behaviors of Ce and Eu frequently observed in REE patterns. A value larger than 1.0 shows that the M-type tetrad effect appears, whereas a value less than 1.0 shows the W-type. In order to express the degree of the tetrad effect by the index, we will mainly employ $(Dy)_{CN}/(Dy^{*})_{CN}$, since the index for Dy should be the most reliable and sensitive indicator of the tetrad effect for the following reasons: (1) the abundance data for Dy are more precise than those for Tb, Tm, and Lu, which means that the index for Dy is better than those for Tb, Tm and Yb; (2) although the index for Pr would be also precise, the tetrad effect appears more distinctively for the third and fourth tetrad probably due to a change in the hydration structure of LREE (Kawabe et al., 1999a).

Chondrite-normalized abundances of Y were plotted on the REE patterns between Dy and Ho by taking account of their ionic radii. If the value of Y is lower than the Ho value in the chondrite-normalized REE pattern, the Y/Ho ratio becomes less than the chondritic value (=28.1). The Y/Ho ratios for most of the granitic rocks examined in this study were almost all

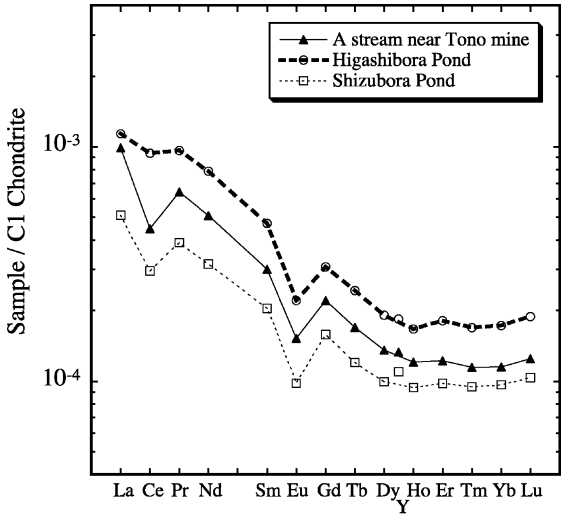


Fig. 7. Chondrite-normalized REE patterns of the surface water around the Tono uranium deposit.

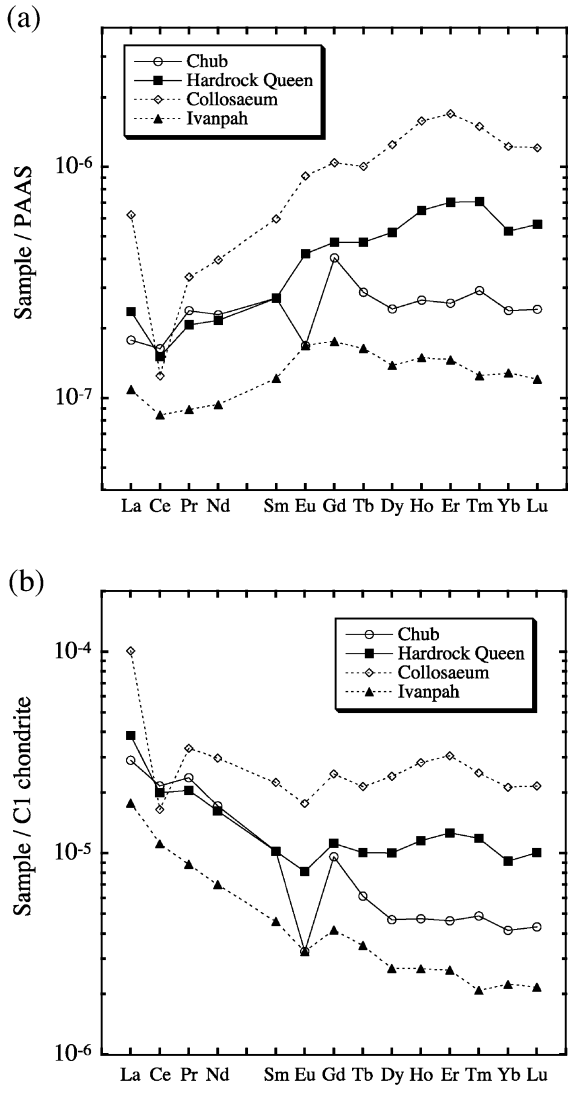


Fig. 8. REE patterns of groundwater from the Mojave Desert (Johannesson et al., 1996) normalized by (a) PAAS (McLennan, 1989) and (b) C1 chondrite.

chondritic. However, some data were lower than the chondritic value, the trend of which is clearer for the granite from the surface outcrops. Cerium anomalies were clearly found in the REE patterns of the granitic rocks from the surface outcrops, but not for the core samples. This reflects the reducing condition of the underground environment from which the core samples were taken. More details on the Ce anomalies of the outcrop samples have been described elsewhere

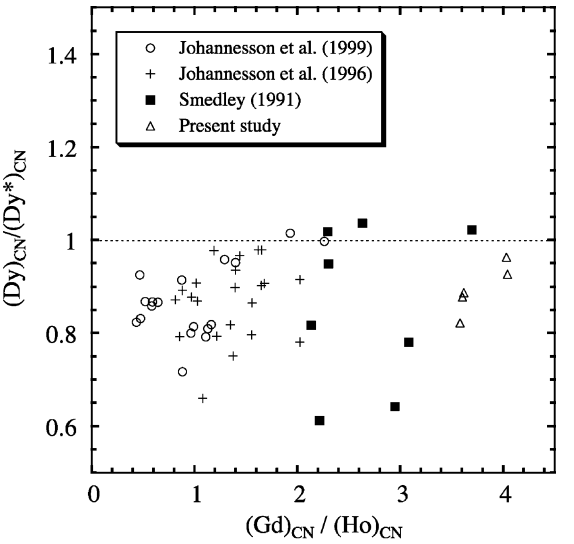


Fig. 9. The relationship between $(Gd)_{CN}/(Ho)_{CN}$ and $(Dy)_{CN}/(Dy^*)_{CN}$ for REE abundances in groundwater reported by Johannesson and Hendry (1999), Johannesson et al. (1996) and Smedley (1991) with data from the present study.

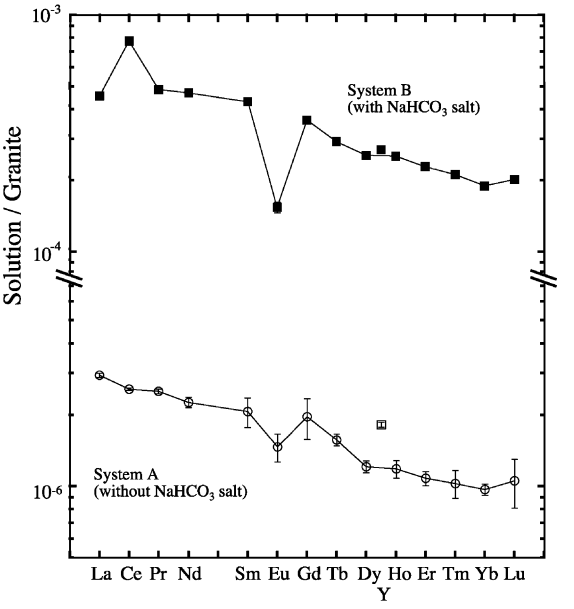


Fig. 10. The distribution coefficient of REE for the leaching experiments. The REE were leached by Milli-Q water from the granitic rock of KNA-6 core at 54.9 m. Two systems in the absence (System A) and presence (System B) of $NaHCO_3$ salt (0.38 mM) were conducted. The REE abundances in the water were normalized by the REE abundances in the corresponding granitic rock.

Table 6
REE and U abundances (ppm) and various indices in the REE patterns of sedimentary rocks obtained from KNA-3 core

| | 31.7 m (coarse) | 31.7 m (fine) | 35.4 m | 38.0 m |
|---|---|---|---|---|
| Y | 55.7 | 42.3 | 28.2 | 34.5 |
| La | 41.3 | 24.1 | 13.6 | 18.3 |
| Ce | 77.9 | 43.5 | 28.2 | 46.1 |
| Pr | 9.13 | 5.37 | 3.65 | 5.24 |
| Nd | 35.6 | 23.4 | 14.9 | 23.4 |
| Sm | 6.79 | 5.26 | 3.60 | 5.35 |
| Eu | 1.77 | 1.55 | 0.694 | 1.54 |
| Gd | 7.33 | 5.71 | 4.19 | 5.88 |
| Tb | 1.26 | 0.932 | 0.675 | 0.920 |
| Dy | 7.75 | 5.75 | 4.24 | 5.84 |
| Ho | 1.79 | 1.28 | 0.899 | 1.24 |
| Er | 5.74 | 4.02 | 2.67 | 3.90 |
| Tm | 0.904 | 0.582 | 0.418 | 0.544 |
| Yb | 6.05 | 4.06 | 2.85 | 3.34 |
| Lu | 1.00 | 0.625 | 0.426 | 0.496 |
| U | 3770 | 3050 | 749 | 13 200 |
| Y/Ho | 31.1 | 33.1 | 31.4 | 27.8 |
| $(Pr)_{CN}/(Pr^*)_{CN}$ | 0.996 | 0.928 | 1.03 | 0.991 |
| $(Tb)_{CN}/(Tb^*)_{CN}$ | 0.974 | 0.956 | 0.957 | 0.935 |
| $(Dy)_{CN}/(Dy^*)_{CN}$ | 0.943 | 0.954 | 0.986 | 0.978 |
| $(Tm)_{CN}/(Tm^*)_{CN}$ | 0.989 | 0.945 | 1.01 | 0.973 |
| $(Yb)_{CN}/(Yb^*)_{CN}$ | 0.942 | 0.975 | 1.01 | 0.947 |

together with the observed oxidation states of Ce (Takahashi et al., 2000).

### 6.2. Groundwater

The REE abundances in the groundwater are listed in Table 5, together with the average values of blank analyses. The blank data were obtained by dividing REE concentration in the blank solution by the preconcentration factor, 100. The blank solution was prepared similarly to the groundwater sample except for the process of eluting groundwater sample into the column. Hence, the blank includes contributions from all reagents and processes for the groundwater analysis. Therefore, the blank data can be treated as our detection limit for the groundwater analysis. The contributions of the blanks have been subtracted from the REE abundances in the groundwaters listed in Table 5. The chondrite-normalized patterns of $REE_{dis}$ and $(REE_{sorb}+REE_{dis})$ in the groundwater from the granitic rocks and from the unconformity in the boreholes KNA-6 and KNA-2, are shown in Fig. 6. It must be noted that the W-type tetrad effects are observed in the REE patterns of the groundwater. In addition, the Y/Ho ratios are larger than the chondritic value. For comparison, $REE_{dis}$ patterns of the surface waters from a stream and two ponds near the Tono mine are also shown in Fig. 7. In these patterns, the tetrad effects are not as clear as those in the REE patterns of groundwaters. In addition, Ce anomalies are clearly observed in their REE patterns in contrast to the REE patterns of the groundwater. This suggests that the groundwater evolved under more reducing conditions than those of the surface water.

Since the precise analysis of REE in groundwater is still not easy, one may question whether the W-type tetrad effect of the groundwater observed in this study is due to experimental errors. However, it is suggested that the W-type tetrad effect is also frequently found in REE abundances of groundwater reported in the literature. In the studies by Johannesson and Hendry (1999) and Johannesson et al. (1996), normalization by 'Average Shale' (Elderfield and Greaves, 1982; De

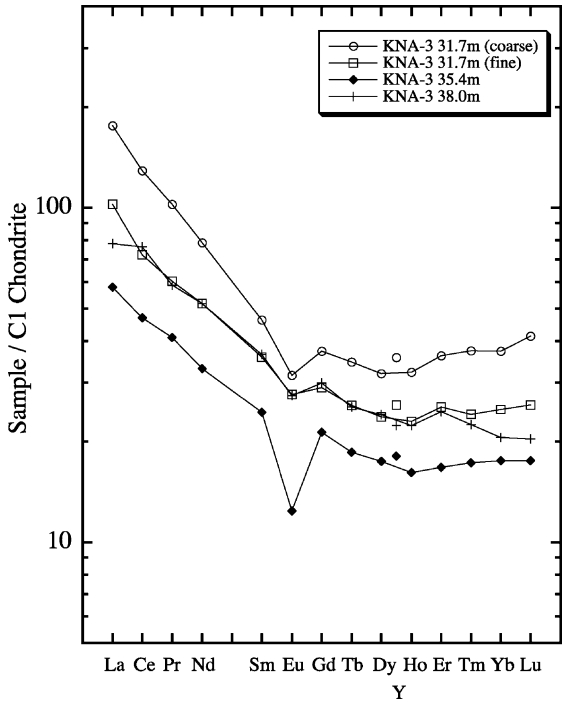


Fig. 11. Chondrite-normalized REE patterns of sedimentary rocks in the Tono uranium deposit.

Baar et al., 1983; Sholkovitz, 1988) was employed for their REE patterns. As noted by McLennan (1994), however, normalization by the Average Shale adds some artifacts to the hyperfine structure of REE patterns, while normalization by PAAS (Average of 23 post-Archean Shales from Australia; McLennan, 1989) is highly recommended. Although tetrad effects are obscure in the REE patterns in Johannesson and Hendry (1999) and Johannesson et al. (1996) due to normalization by the Average Shale, normalization by PAAS obviously shows W-type tetrad effects especially in the third tetrad (Gd–Tb–Dy–Ho span) in their groundwater data (Fig. 8a). Since relative abundances of REE in PAAS against C1 chondrite show a smooth pattern (McLennan, 1994), the normalization by C1 chondrite conducted in this study will preserve hyperfine structures in REE patterns, like W-type tetrad effects for groundwater (Fig. 8b). To compare REE patterns from the literature with our data objectively (without selecting literature values subjectively), all $(Dy)_{CN}/(Dy^*)_{CN}$ for the REE abundances in the studies by Johannesson and Hendry (1999), Johannesson et al. (1996) and Smedley (1991) were plotted against $(Gd)_{CN}/(Ho)_{CN}$ ratios together with our data (Fig. 9). Irrespective of the local slope of REE pattern inferred from $(Gd)_{CN}/(Ho)_{CN}$, most $(Dy)_{CN}/(Dy^*)_{CN}$ values were less than 1, suggesting the appearance of W-type tetrad effects commonly found in groundwater samples. Based on these results, it is quite natural that the W-type tetrad effects are also found in our groundwater samples.

Stetzenbach et al. (1994) reported Y abundance in groundwater in addition to other REE, which enabled us to calculate Y/Ho ratios for their groundwater data. The Y/Ho ratios in their groundwaters (three samples) were 67.8, 71.4, and 104, showing that Y/Ho ratios deviated from the chondritic value (=28.1) to a great degree. The results are also similar to what we found in this study.

The concentration of U in the groundwater at the unconformity in borehole KNA-6 was also measured (Table 3), and was found to be lower than that of the groundwater from the granite. This is consistent with the different redox potentials of these two waters. The

Table 7
REE abudances (ppm), various indices in REE pattern, and $(^{234}U)_{ac}/(^{238}U)_{ac}$ in U minerals in the sedimentary rocks of the Tono uranium deposit measured by SIMS

| | Biotite I | Biotite II | Clay mineral I | Clay mineral II | Pyrite I | Pyrite II |
|---|---|---|---|---|---|---|
| Y | 2150 | 5200 | 11400 | – | 3040 | – |
| La | 335 | 485 | 1280 | – | 309 | – |
| Ce | 1200 | 1460 | 6350 | – | 1450 | – |
| Pr | 185 | 263 | 1030 | – | 205 | – |
| Nd | 1210 | 1430 | 7040 | – | 1580 | – |
| Sm | 202 | 306 | 1440 | – | 385 | – |
| Eu | 32.0 | 41.6 | 213 | – | 55.3 | – |
| Gd | 181 | 222 | 1070 | – | 279 | – |
| Tb | 19.3 | 27.8 | 144 | – | 45.1 | – |
| Dy | 126 | 203 | 926 | – | 310 | – |
| Ho | 31.8 | 53.2 | 209 | – | 67.1 | – |
| Er | 90.0 | 169 | 634 | – | 203 | – |
| Tm | 13.5 | 27.4 | 100 | – | 37.1 | – |
| Yb | 82.6 | 231 | 650 | – | 289 | – |
| Lu | 15.2 | 41.2 | 131 | – | 48.5 | – |
| ΣREE | 3724 | 12600 | 40300 | – | 10300 | – |
| Y/Ho | 67.6 | 97.7 | 54.4 | – | 45.3 | – |
| $(Pr)_{CN}/(Pr^*)_{CN}$ | 0.958 | 1.07 | 1.06 | – | 0.913 | – |
| $(Tb)_{CN}/(Tb^*)_{CN}$ | 0.676 | 0.716 | 0.827 | – | 0.924 | – |
| $(Dy)_{CN}/(Dy^*)_{CN}$ | 0.774 | 0.828 | 0.897 | – | 1.00 | – |
| $(Tm)_{CN}/(Tm^*)_{CN}$ | 0.954 | 0.914 | 0.939 | – | 1.03 | – |
| $(Yb)_{CN}/(Tb^*)_{CN}$ | 0.840 | 0.981 | 0.819 | – | 1.04 | – |
| $(^{234}U)_{ac}/^{238}U)_{ac}$ | 1.32 ± 0.03 | 0.98 ± 0.03 | 0.83 ± 0.01 | 0.95 ± 0.02 | 1.11 ± 0.01 | 0.98 ± 0.02 |

water from the unconformity close to the sedimentary rocks is relatively reducing, thereby decreasing the concentration of dissolved U(VI) owing to reduction to insoluble U(IV) species.

### 6.3. Leaching experiments

Logarithms of REE distribution coefficients, the ratio between REE concentrations leached by Milli-Q water and those in the granitic rocks, are plotted in Fig. 10. In the presence of carbonate (system B), REE were more leachable by over two orders of magnitude, probably due to the formation of REE-carbonate complex ions in the aqueous phase. Similar results were reported for leaching experiments for basalt (Minami et al., 1995). In the distribution patterns, the W-type tetrad curves were observed in all systems, as was also reported by Minami et al. (1995). The Y/Ho ratios in the absence of $NaHCO_3$ salt (systems A) showed clearly larger values than the chondritic value, whereas the value in the presence of $NaHCO_3$ salt (system B) was slightly larger than the chondritic value. An anomalous Ce value was found in the pattern of system B probably due to the formation of Ce(IV) polycarbonate complexes which can be found under alkaline and carbonate-rich condition (Möller and Bau, 1993).

### 6.4. Sedimentary rocks (whole rock analysis and analysis for U-mineralized zone by SIMS)

The sedimentary rocks examined consist of various types of rocks, such as conglomerate, tuffaceous rock including clastic minerals and lignite, sandstone, and mudstone. Some descriptions and major element compositions of the sedimentary rocks are summarized in Table 2. The major element compositions show that the sedimentary rocks are quite heterogeneous. In Table 6, REE abundances in sedimentary rocks (whole rock) are shown, and the corresponding chondrite-normalized patterns exhibit the W-type tetrad effects (Fig. 11). In addition, Y/Ho ratios were slightly larger than the chondritic value for these sedimentary rocks.

The REE abundances and the chondrite-normalized patterns in the U-mineralized zone of the sedimentary rocks (KNA-3 at 31.7 m depth, coarse grained part) are shown in Table 7 and Fig. 12. Four

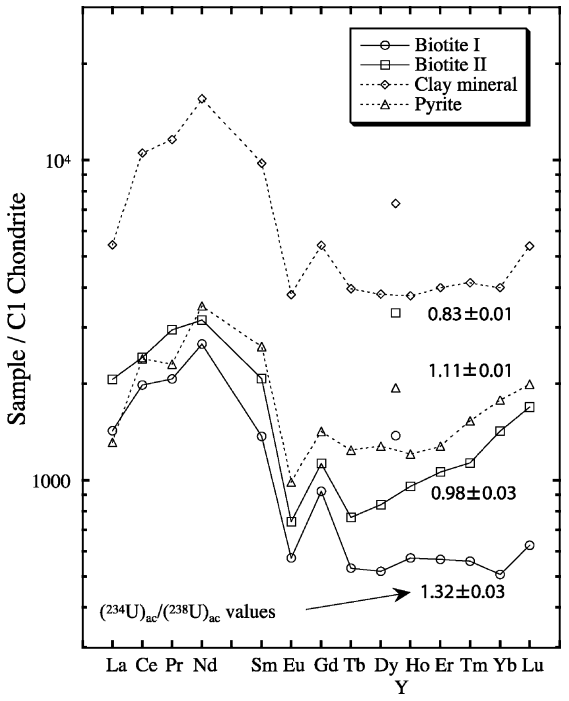


Fig. 12. Chondrite-normalized REE patterns of the U-mineralized zone in the sedimentary rocks of KNA-3 at 31.7 m depth (coarse grain part) investigated by SIMS. The activity ratios of $^{234}U$ and $^{238}U$ determined by SIMS are also shown.

U-mineralized zones formed in the cleavage of biotite, clay minerals, and at the margin of pyrite, were analyzed after identifying the minerals by EPMA. The total amount of all the REE in the U minerals was large, even reaching 1% in some analyses. This indicates that REE behavior is closely related to U behavior. The analyses of Ce, Pr, and Nd may have large errors due to the heterogeneity of their abundances in the standard uraninite. Relative standard deviations of repeated analyses for Ce, Pr, and Nd abundances in the standard uraninite determined by ICP-MS (Fig. 4) were 27%, 11%, and 12%, respectively, while it was less than 10% for the other REE. In spite of such uncertainty, enrichment of Pr, Nd, or Sm in the chondrite-normalized REE patterns of the U-mineralized zone was clearly observed. This feature has often been found in the REE patterns of uraninite as shown by Hidaka et al. (1992). From the HREE region, we can discuss the fractionation of HREE from the viewpoint of the tetrad effect and Y/Ho ratio.

Most of the REE patterns in Fig. 12 exhibit W-type tetrad curves in their third (Gd–Tb–Dy–Ho span) and fourth tetrad (Er–Tm–Yb–Lu span) except for the spot of pyrite; Y/Ho ratios for these four U-mineralized zones were far above the chondritic value.

## 7. Discussion

### *7.1. Weathering of the granitic rocks and their REE patterns*

The CIA values varied from 52 to 61 for the granite rocks from the surface outcrops. Although the granitic rocks from core samples (KNA-6 and BH-1) were quite friable, their CIA values ranged from 49 to 53. The values are lower than those for the granitic rocks from the surface outcrop, which ranged from 52 to 61. This suggests that the weathering mechanism is somewhat different between the ground surface and underground environment, and that the CIA values are not effective indices of the degree of weathering in the core samples. The relation between CIA and porosity ($n_p$) is shown in Fig. 13. These two values have a positive correlation, although $n_p$ is more variable for the samples from drilling cores that show relatively lower CIA values. The $n_p$ values for some granitic rocks from the core (KNA-6 at 6.7 and 54.9 m points) reached as much as 30%. Generally, $n_p$ increases as a result of weathering in the granitic rock (e.g., Maynard et al., 1994). This allows us to estimate the degree of weathering in the granitic rocks by using $n_p$ as a measure for the core samples in the following discussion.

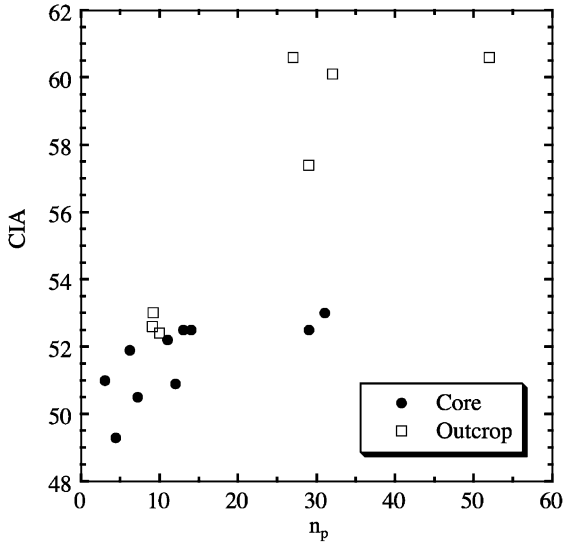


Fig. 13. The relationship between CIA and porosity ($n_p$) for the Toki granitic rocks obtained from drilling cores and surface outcrop.

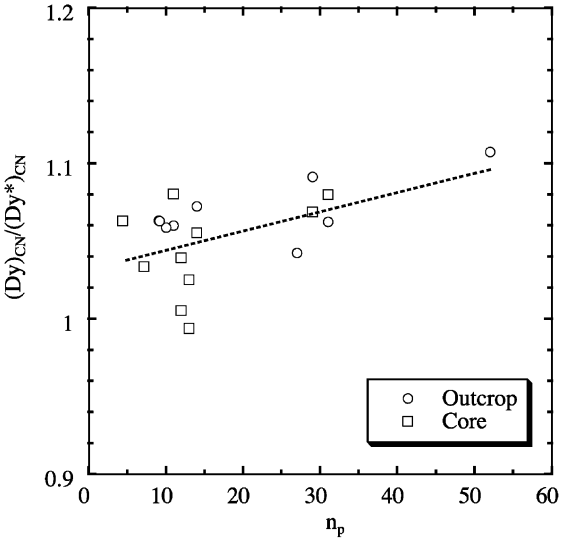


Fig. 14. The relationship between $n_p$ and degrees of tetrad effects (Dy/Dy*) for the Toki granitic rock obtained from drilling cores and surface outcrop. The dotted line shows a regression line ($r = 0.53$).

An obvious feature of the REE patterns of the granitic rocks is their M-type tetrad effects. The prominence of the tetrad effect obtained by Eq. (4) (Table 4) was plotted against $n_p$ by using $(Dy)_{CN}/(Dy^*)_{CN}$ as an index of the effect in Fig. 14, which shows a weak correlation ($r = 0.53$). Some samples showing lower $n_p$ values do not show the tetrad effect, whereas sample with higher $n_p$ values show the tetrad effect. This may show that the larger M-type tetrad effect occurs in more weathered samples and that the M-type tetrad effects in the granitic rocks were produced during weathering processes. Many studies of REE behavior in the weathering processes have shown that REE are rather mobile during weathering (e.g., Nesbitt, 1979; Condie et al., 1995). Thus, the M-type tetrad effects can reasonably occur in the granitic rocks as a result of water–rock interaction.

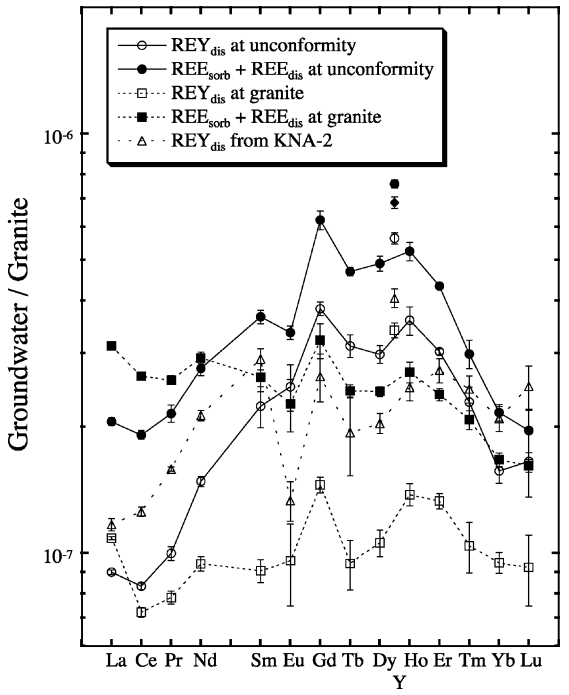


Fig. 15. REE patterns of the groundwater normalized by the granitic rock from the vicinity of the groundwater sampling point.

### 7.2. REE tetrad effect and non-chondritic Y/Ho ratio during granite–groundwater interaction

The groundwater in the granitic rocks is generally of $Na^+$–$HCO_3^-$ type; more details of the chemical compositions of groundwater in the granite were reported in Iwatsuki and Yoshida (1999). Their results showed that the groundwater has evolved during water–rock interaction with the granitic rocks. In the REE patterns of the groundwaters, the W-type tetrad effects are more clearly observed compared with those in the surface waters (Figs. 6 and 7). The granitic rocks show the M-type tetrad effects (Fig. 5a), while the W-type tetrad effects, the counterpart of the fractionation, were generated in the REE patterns of the groundwater (Fig. 6). The simultaneous observation of conjugate M- and W-type tetrad effects for the granitic rocks and groundwater supports the hypothesis that these tetrad effects were brought about by water–rock interactions in the Tono area. The Y/Ho ratios in the groundwater are also much larger than the chondritic value, whereas the ratios for the granitic rocks were similar to or slightly less than the chondritic value. This seems consistent with the simultaneous appearance of M- and W-type tetrad effects in the granitic and groundwater, respectively.

The REE fractionation caused by the tetrad effect during the water–rock interaction is more clearly recognized by normalizing the REE patterns of the groundwater by the REE values of granitic rocks from near the sampling site of the groundwater (Fig. 15). This shows that in addition to the third and fourth tetrads, the tetrad effect can also be recognized in the first tetrad (La–Ce–Pr–Nd span). The REE abundances in the aqueous phase relative to those in the granitic rock (at 54.9 m in KNA-6) were obtained from the leaching experiments (Fig. 10). The presence of carbonate ions evidently increased the REE fraction in the aqueous phase. This is due to the formation of REE–carbonate complex in the aqueous phase as will be shown in Section 7.3. Both in the presence and absence of carbonate, W-type tetrad effects were ob-

Table 8
Speciation calculation of dissolved species of Ln (Ln = Ce, Gd) in the Tono groundwater estimated from their stability constants at I = 0

| | Ce species (%) | Gd species (%) | References for stability constants |
|---|---|---|---|
| $Ln^{3+}$ | $3 \times 10^{-4}$ | $5 \times 10^{-5}$ | – |
| $LnCO_3^+$ | 2.1 | 0.83 | Lee and Byrne (1993) |
| $Ln(CO_3)_2^-$ | 86.3 | 83.6 | Lee and Byrne (1993) |
| $LnPO_4$ | 11.6[a] | 15.5[a] | Byrne et al. (1991) |
| $LnOH^{2+}$ | $4 \times 10^{-4}$ | $2 \times 10^{-4}$ | Baes and Mesmer (1986) |
| $Ln(OH)_2^+$ | – | $2 \times 10^{-4}$ | Baes and Mesmer (1986) |

Ligand concentrations in the groundwater ($[CO_3^{2-}] = 4 \times 10^{-4}$ mol/dm$^3$; $[PO_4^{3-}] < 2.1 \times 10^{-6}$ mol/dm$^3$; $[OH^-] = 10^{-5.5}$) were reported in Iwatsuki and Yoshida (1999), Japan Nuclear Cycle Development Institute (1996), and Table 3.

[a] Note that $[PO_4^{3-}]$ concentration reported as an upper limite was employed for this calculation. Thus, the calculated results show a possible maximum value for phosphate complex.

served in the leached solution. This also supports the hypothesis that the M-type tetrad effect can be brought about in the granitic rock by contact with groundwater. The Y/Ho ratios were larger than the chondritic value in the aqueous phase in leaching experiments. Based on these results, it is reasonable to suggest that conjugate W- and M-type tetrad effects and non-chondritic Y/Ho ratios can occur in the groundwater and the granitic rocks as a result of water–rock interactions.

In order to evaluate whether it is reasonable to suggest that weathering processes can affect the REE signatures of the granitic rocks to the observed extent, we undertook calculations of mass balance for the water–rock interaction between the groundwater and the granitic rocks. Total REE leached from the granitic rock can be obtained by estimating the groundwater volume ($V_{gw}$) that has passed through a unit volume of granite by:

$$V_{gw} = n_p K R_g T A,$$

where $K$ (cm/s) is hydraulic conductivity; $R_g$, hydraulic gradient; $T$ (s), circulation time; $A$ (cm$^2$), unit surface area (i.e., $A=1$). For the purpose of the scoping calculations, it was assumed that hydraulic conditions have remained similar to the present. The $K$ value ranges from $5.7 \times 10^{-8}$ to $3.6 \times 10^{-5}$ cm/s (Yanagisawa et al., 1991) and $R_g$ from 0.02 to 0.05 (Japan Nuclear Cycle Development Institute, 2000) in the present water–rock system. For $T$, the age of the Toki granite (68 Ma; Suzuki and Adachi, 1998) is employed. The $n_p$ value is fixed at 29%, $n_p$ for KNA-6 core at 54.9 m. From $V_{gw}$ and REE abundances in the groundwater, we can estimate $REE_{leach}$, the total amount of REE leached from a unit volume of granite. The REE data for unfiltered groundwater from granite was employed, since REE can be transported not only as dissolved species but also as sorbed species on particulate matter. The $REE_{leach}$ was divided by the density of granite ($=2.6$ g/cm$^3$ for KNA-6 samples) in order to compare the $REE_{leach}$ directly with REE abundances in the granite. The results are shown in Fig. 16, where the possible region of $REE_{leach}$ estimated as a fraction originally contained in the granite is shown by the shaded area. The large range of the area is mainly caused by the variation of $K$ values found in the granitic rocks. The upper region of the $REE_{leach}$ area is comparable with the present REE

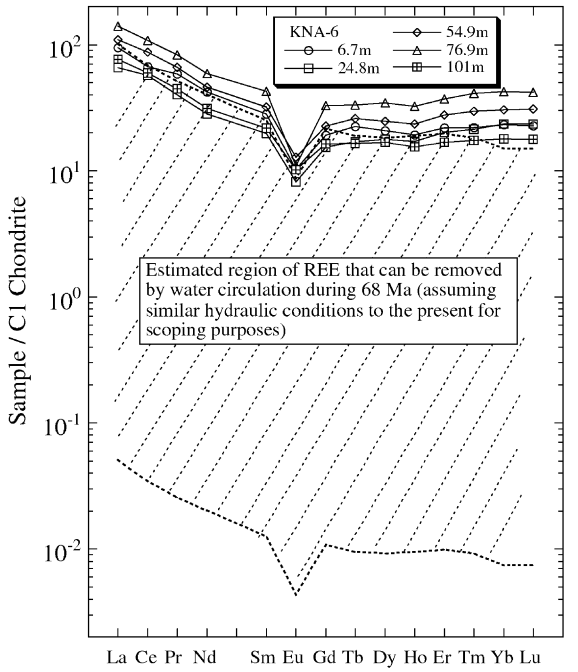


Fig. 16. The REE fractions that could have been leached from granite by water–rock interaction by calculating the total volume of groundwater that could have interacted with the granite under the following conditions. Hydraulic conductivity: $5.7 \times 10^{-8}$ to $3.6 \times 10^{-5}$ cm/s; hydraulic gradient: 0.02 to 0.05; reaction duration: $6.8 \times 10^7$ years; REE abundances in groundwater: REE in unfiltered groundwater at unconformity determined in this study (Table 5); porosity ($n_p$): 29%.

abundances in the granitic rocks, showing that the water–rock interaction could have plausibly altered the REE patterns of the granitic rock at the Tono area. However, it is also probable that the appearance of the M-type tetrad effect was not only produced by low-temperature water–rock interaction with groundwater. An alternative possibility is that REE fractionation during a late stage of granite crystallization has also contributed to induce the M-type tetrad effect (Irber, 1999). Further study is needed to evaluate precisely the magnitude of the weathering needed to produce the tetrad effect in the weathered granitic rocks. However, it is suggested that the water–rock interaction with the groundwater has contributed, more or less, to the formation of the M-type tetrad effects in the granitic rocks, since the W-type tetrad effect was observed in the groundwater, the counterpart of the water–rock system.

### 7.3. REE species in the groundwater

The REE species dissolved in the groundwater were estimated by an equilibrium model (Wood, 1990; Lee and Byrne, 1992, 1993; Stumm and Morgan, 1996). The groundwater of the Tono area contains relatively high concentrations of carbonate ions (Table 3). With such high content of carbonate and high pH, it is considered that REE in the aqueous phase are dissolved mainly as REE–carbonate complex ions ($[REE-(CO_3)^+]$ and $[REE-(CO_3)_2^-]$). This is estimated from the speciation calculation as shown in Table 8 for $Ce^{3+}$ and $Gd^{3+}$. This shows that carbonate complexes are dominant for their dissolved species, while phosphate complexes are at most 16% (note that the phosphate ion concentration used for the calculation was reported only as an upper limit value). Contribution of hydrolysis is far less important. It has been recognized that the solid–water equilibrium determined by the formation of carbonate complexes in the aqueous phase at pH above neutral brings about the W-type tetrad effect in the aqueous phase as observed in seawater and groundwater (Masuda and Ikeuchi, 1979; Masuda et al., 1987; Kawabe, 1992; Kawabe et al., 1998). Theoretical treatments with laboratory experiments (Kawabe et al., 1999b; Ohta and Kawabe, 2000) support that the equilibrium between dissolved REE–carbonate complex and REE in the solid phase such as REE sorbed on colloidal materials and REE in the oxides can produce the W-type tetrad effect in the aqueous phase. Although we do not refer to the details here, the fact is consistent with the present results on the appearance of W-type tetrad effect in the Tono groundwater.

### 7.4. REE patterns in the sedimentary rocks and U mineralized zone

The REE patterns of the sedimentary rocks showed W-type tetrad effects and relatively larger Y/Ho ratios (Fig. 11). This suggests that the W-type tetrad effects and larger non-chondritic Y/Ho ratios in the sedimentary rocks resulted from the modification of their original patterns by REE provided from groundwater.

The REE abundances in the U-mineralized zone (Fig. 12) showed enrichment of REE in the U-bearing mineral, slight W-type tetrad effects, and larger Y/Ho ratios than the chondritic value. These results indicate that the REE in the U-mineralized zone were transported by the groundwater, which agrees with our estimation based on the whole-rock analyses of the sedimentary rocks. Let us consider the dilution of a U mineral with Y/Ho = 66 and Ho = 90 ppm (average values of REE in U mineral determined by SIMS) by sedimentary rocks having chondritic Y/Ho ratio (= 28) and Ho = 1.8 ppm (= the value of KNA-6 at 31.7 m, coarse grained part). If we dilute the U mineral until we obtain the U concentration of the sedimentary rock (= 3770 ppm in the sample of KNA-6 at 31.7 m, coarse grained part), the Y/Ho ratio will be 33. This is rather consistent with the Y/Ho value of 31.1 for a sample from KNA-6 at 31.7 m (coarse grained part). This result implies that the Y/Ho ratio slightly larger than the chondritic value in the sedimentary rocks may be due to the large Y/Ho value in the U-mineralized part.

We could successfully detect $^{234}U$ to obtain $(^{234}U)_{ac}/(^{238}U)_{ac}$ in the U-mineralized zone (Table 7 and Fig. 12). The values, varying from 0.83 to 1.32, show that uranium disequilibrium is found in the U-mineralized zone. Any departure of $(^{234}U)_{ac}/(^{238}U)_{ac}$ from unity is usually due to water–rock interaction (Kigoshi, 1971). In such processes, $^{234}U$ in the solid phase is more preferentially dissolved into the aqueous phase than $^{238}U$, because of damage to the crystal lattice by α-recoil energy in the vicinity of $^{234}U$ which may happen in U leaching from granite in Tono area (Kigoshi, 1971). However, during fixation in the solid phase, we can assume that the behaviors of $^{234}U$ and $^{238}U$ are similar, and the ratio is kept constant in the fixation process. Therefore, a value greater than unity shows the formation of the U-mineralization from groundwater, while a value less than unity indicates that U has been removed secondarily from the U-mineralized zone within a period shorter than above five times of $^{234}U$'s half life (= 1.2 million years). Yoshida et al. (1994) analyzed the ratio for various host minerals that contain a large amount of U (e.g., biotite, pyrite etc.) by an α-counting method after mineral separation. Their results are consistent with the present ones, obtained by measuring the U-mineralized zone directly by SIMS. Such a U disequilibrium study shows that U in the U-mineralized zone was deposited from groundwater, while the ratio less than 1 shows that U was secondarily removed from U-mineralized zone after

the U deposition. It is worthy of note that the REE pattern shown in Fig. 12 was obtained from the same part of the U-mineralized zone that shows U disequilibrium. Therefore, the result confirms that REE in the groundwater were incorporated into the U-mineralized zone in the sedimentary rocks.

## 8. Conclusion—systematics of the tetrad effects and Y/Ho ratios observed in the Tono area and their implications

Table 9 summarizes the averaged values of Y/Ho ratios and the magnitudes of tetrad effects for the weathered granitic rocks obtained from core samples (KNA-6 and BH-1), the groundwater with and without particulate matter, the sedimentary rocks, and its U-mineralized zone. It should be noted that conjugate W- and M-type tetrad effects were observed in the Tono area. The variation of Y/Ho ratios was consistent with that of the magnitude of the tetrad effect. The latter, expressed by $(Dy)_{CN}/(Dy^*)_{CN}$, was plotted against the Y/Ho ratio for the granitic rocks, the groundwater with and without particulate matter, the sedimentary rocks, and the U-mineralized zone (Fig. 17). These results allow us to speculate the migration of REE in the Tono area. The groundwater leaches REE from the granitic rocks, where W-type tetrad effects and higher Y/Ho ratios than chondrite are produced in the groundwater. The weathered granitic rocks, the residue of the water–rock interaction, exhibit M-type tetrad effects and slightly lower Y/Ho ratios. The REE in the U-mineralized zone preserve W-type tetrad effects and higher Y/Ho ratios, transmitted from groundwater. This influences the REE pattern of the bulk sedimentary rocks, which consequently have W-type tetrad effects and slightly higher Y/Ho ratios. In these processes, the preference of groundwater for W-type tetrad effects and larger Y/Ho ratios is primarily responsible for producing REE variations in the granitic rocks and the sedimentary

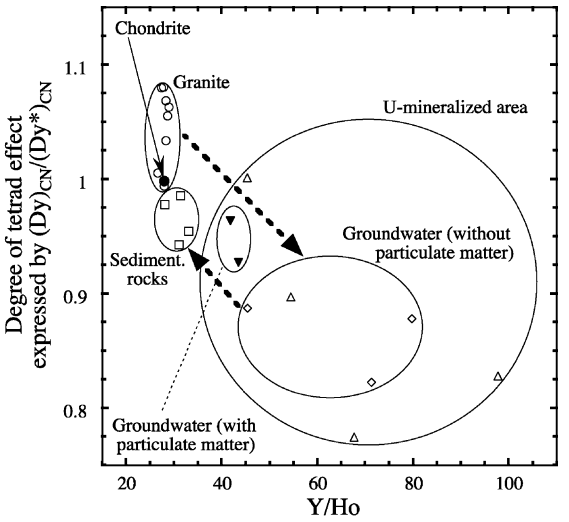


Fig. 17. The relationship between Y/Ho ratios and the magnitudes of the tetrad effects expressed by $(Dy)_{CN}/(Dy^*)_{CN}$ in the Tono area. These results suggest that REE leached from the granitic rocks are transported by groundwater to the sedimentary rocks. See text for details.

Table 9
The averaged values of degrees of tetrad effects and Y/Ho ratios for weathered granite obtained from cores (KNA-6 and BH-1), groundwater, REE sorbed on particulate matter, sedimentary rocks, and U minerals from sedimentary rock at 31.7 m depth (coarse grained part) of KNA-3 core

| | Granite | | Groundwater (without particulate matter)[a] | | Groundwater (with particulate matter)[b] | | Sedimentary rock | | U mineral (KNA-3 31. 7 m, coarse grain part) | |
|---|---|---|---|---|---|---|---|---|---|---|
| | Average | $\sigma$ | Average | $\sigma$ | Average | $\sigma$ | Average | $\sigma$ | Average | $\sigma$ |
| Y/Ho | 28.0 | 0.7 | 65.5 | 13.2 | 42.6 | – | 30.9 | 2.1 | 66.3 | 22.9 |
| $(Pr)_{CN}/(Pr^*)_{CN}$ | 1.06 | 0.02 | 0.894 | 0.019 | 0.926 | – | 0.986 | 0.051 | 1.00 | 0.07 |
| $(Tb)_{CN}/(Tb^*)_{CN}$ | 1.07 | 0.06 | 0.850 | 0.035 | 0.911 | – | 0.955 | 0.013 | 0.786 | 0.087 |
| $(Dy)_{CN}/(Dy^*)_{CN}$ | 1.05 | 0.03 | 0.862 | 0.051 | 0.945 | – | 0.965 | 0.016 | 0.875 | 0.073 |
| $(Tm)_{CN}/(Tm^*)_{CN}$ | 1.02 | 0.03 | 0.942 | 0.052 | 0.974 | – | 0.981 | 0.035 | 0.960 | 0.052 |
| $(Yb)_{CN}/(Yb^*)_{CN}$ | 1.03 | 0.03 | 0.840 | 0.040 | 0.884 | – | 0.970 | 0.034 | 0.919 | 0.093 |

[a] Obtained from the values for ($REE_{dis}$) defined in Section 4.3.
[b] Obtained from the values for ($REE_{sorb} + REE_{dis}$) defined in Section 4.3.

rocks in the Tono area, from which we can assess the REE behavior. Irrespective of these systematic variation of Dy/Dy*, further study is needed for the points below. Firstly, we need to be careful to discern the extent of tetrad effect in REE patterns if it is slightly observed. Secondly, we need to quantify the contribution of the effect through granite crystallization at its late stage to the degree of M-type tetrad effect found in granite samples.

In summary, based on the variation in the tetrad effect and Y/Ho ratios, it is considered that REE leached from the granitic rocks are transported by groundwater to the sedimentary rocks, and then incorporated into the U-mineralized zone. These results may support the conclusions from previous studies about mass transfer of U in the Tono, namely that U was leached from the granitic rocks and then precipitated in the sedimentary rocks after being transported by groundwater. The present study suggests that the degree of the tetrad effect and the variation of Y/Ho ratios observed in the REE patterns are promising tools to understand the water–rock interactions affecting the migration of REE and related elements (e.g., U).

## Acknowledgements

We are greatly indebted to Dr. R. Metcalfe of British Geological Survey (JNC international fellowship) for his critical review on this work. We thank Prof. H. Hidaka (Hiroshima University) for providing uraninite standard samples and for his constructive comments. Great thanks are due to T. Kunimaru (JNC) for his help on the ICP-MS measurement. We also thank Prof. Y. Sano and Dr. K. Terada (Hiroshima University) for their advice on SIMS analyses. Thanks are extended to T. Shibata and H. Ishisako for their great assistance to this work. Finally, we thank S.A. Wood and M. Bau for their thorough and constructive reviews. **JD**

## References

Anders, E., Grevesse, N., 1989. Abundances of the elements: meteoritic and solar. Geochim. Cosmochim. Acta 57, 197–214.

Aubert, D., Stille, P., Probst, A., 2001. REE fractionation during granite weathering and removal by waters and suspended loads: Sr and Nd isotopic evidence. Geochim. Cosmochim. Acta 65, 387–406.

Baes Jr., C.F., Mesmer, R.E., 1986. The Hydrolysis of Cations. Krieger Publishing, Florida.

Bau, M., 1996. Controls on the fractionation of isovalent trace elements in magmatic and aqueous systems: evidence from Y/Ho, Zr/Hf, and lanthanide tetrad effect. Contrib. Mineral. Petrol. 123, 323–333.

Bau, M., Usui, A., Pracejus, B., Mita, N., Kanai, Y., Irber, W., Dulski, P., 1998. Geochemistry of low-temperature water–rock interaction: evidence from natural waters, andesite, and iron–oxyhydroxide precipitates at Nishiki-numa iron-spring, Hokkaido, Japan. Chem. Geol. 151, 293–307.

Byrne, R.H., Lee, J.H., Bingler, L.S., 1991. Rare earth elements complexation by OP43-ions in aqueous solution. Geochim. Cosmochim. Acta 55, 2729–2735.

Condie, K.C., Dengate, J., Cullers, R.L., 1995. Behavior of rare-earth elements in a paleoweathering profile on granodiorite in the front range, CO, USA. Geochim. Cosmochim. Acta 59, 279–294.

Doi, K., Hirono, S., Sakamaki, Y., 1975. Uranium mineralization by ground water in sedimentary rocks, Japan. Econ. Geol. 70, 628–646.

De Baar, H.J.W., Bacon, M.P., Brewer, P.G., Bruland, K.W., 1983. Rare earth distribution with a positive Ce anomaly in the western Atlantic Ocean. Nature 301, 324–327.

De Baar, H.J.W., Bacon, M.P., Brewer, P.G., Bruland, K.W., 1985. Rare earth elements in the Pacific and Atlantic oceans. Geochim. Cosmochim. Acta 49, 1943–1959.

Elderfield, H., Greaves, M.J., 1982. The rare earth elements in seawater. Nature 296, 214–219.

Hanamuro, T., Ota, K., Yoshida, H., 1995. Study of nuclide migration in sedimentary rocks at the Tono Uranium Deposit—characteristics of flow-path structure in relation to nuclide sorption and retardation. Donen Gihou 93, 53–61 (in Japanese).

Henderson, P., 1984. Rare Earth Element Geochemistry. Elsevier, Amsterdam.

Hidaka, H., Holliger, P., Shimizu, H., Masuda, A., 1992. Lanthanide tetrad effect observed in the Oklo and ordinary uraninites and its implication for their forming processes. Geochem. J. 26, 337–346.

Holliger, P., 1988. Ages U–Pb definis in situ sur osydes D'urenium a l'analyseur ionique: methodologie et consequences geochimiques. C. R. Acad. Sci. Paris 307, 367–373.

Imai, N., Terashima, S., Itoh, S., Ando, A., 1995. 1994 compilation values for GSJ reference samples, "Igneous rock series". Geochem. J. 29, 91–95.

Irber, W., 1999. The lanthanide tetrad effect and its correlation with K/Rb, Eu/Eu*, Sr/Eu, Y/Ho, and Zr/Hf of evolving peraluminous granite suites. Geochim. Cosmochim. Acta 63, 489–508.

Ishihara, S., Suzuki, Y., 1969. Basement granites of the Toki uranium deposits in Tono region. Rep. Geol. Surv. Jpn. 232, 113–128.

Iwatsuki, T., Yoshida, H., 1999. Groundwater chemistry and fracture mineralogy in the basement granitic rock in the Tono Uranium mine area, Gifu Prefecture, Japan — Groundwater composition,

Eh evolution analysis by fracture filling minerals. Geochem. J. 33, 19–32.

Japan Nuclear Cycle Development Institute, 1996. Tono Natural Analogue Programme Technical Note 96-01, PNC TE0076 97-007.

Japan Nuclear Cycle Development Institute, 2000. H12: Project to Establish the Scientific and Technical Basis for HLW Disposal in Japan. JNC TN1400 99-020.

Johannesson, K.H., Hendry, M.J., 1999. Rare earth elements geochemistry of groundwaters from a thick till and clay-rich aquitard sequence, Saskatchewan, Canada. Geochim. Cosmochim. Acta 64, 1493–1509.

Johannesson, K.H., Stetzenbach, K.J., Hodge, V.F., Lyons, W.B., 1996. Rare earth elements complexation behavior in circumneutral pH groundwaters: assessing the role of carbonate and phosphate ions. Earth Planet Sci. Lett. 139, 305–319.

Kagi, H., Dohmoto, Y., Takano, S., Masuda, A., 1993. Tetrad effect in lanthanide partitioning between calcium sulfate crystal and its saturated solution. Chem. Geol. 107, 71–82.

Katayama, N., Kamiya, T., 1977. Favorable conditions for the formation of basal type uranium deposits. Min. Geol. 27, 1–8.

Katayama, N., Kubo, K., Hirono, S., 1974. Genesis of uranium deposits of the Tono Mine, Japan. Proc. IAEA-SH-183/11, pp. 437–452.

Kawabe, I., 1992. Lanthanide tetrad effect in the $Ln^{3+}$ ionic radii and refined spin-paring energy theory. Geochem. J. 26, 309–335.

Kawabe, I., 1999. Hydration change of aqueous lanthanide ions and tetrad effects in lanthanide(III)–carbonate complexation. Geochem. J. 33, 267–275.

Kawabe, I., Kitahara, Y., Naito, K., 1991. Non-chondritic yttrium/holmium ratio and lanthanide tetrad effect observed in pre-Cenozoic limestones. Geochem. J. 25, 31–44.

Kawabe, I., Toriumi, T., Ohta, A., Miura, N., 1998. Monoisotopic REE abundances in seawater and the origin of seawater tetrad effect. Geochem. J. 32, 213–229.

Kawabe, I., Ohta, A., Ishii, S., Tokumura, M., Miyauchi, K., 1999a. REE partitioning between Fe–Mn oxyhydroxide precipitates and weakly acid NaCl solutions: convex tetrad effect and fractionation of Y and Sc from heavy lanthanides. Geochem. J. 33, 167–179.

Kawabe, I., Ohta, A., Miura, N., 1999b. Distribution coefficients of REE between Fe oxyhydroxide precipitates and NaCl solutons affected by REE–carbonate complexation. Geochem. J. 33, 181–197.

Kigoshi, K., 1971. Alpha-recoil thorium-234: dissolution into water and the uranium-234/uranium-238 disequilibrium in nature. Science 173, 47–48.

Kish, L., Cuney, M., 1981. Uraninite–albite veins from the Mistamisk Valley of the Labrador Trough, Quebec. Min. Mag. 44, 471–483.

Langmuir, D., 1978. Uranium-solution mineral equilibria at low-temperatures with applications to sedimentary ore deposits. Geochim. Cosmochim. Acta 42, 547–569.

Lee, J.H., Byrne, R.H., 1992. Examination of comparative rare earth elements complexation behavior using linear free-energy relationships. Geochim. Cosmochim. Acta 56, 1127–1137.

Lee, J.H., Byrne, R.H., 1993. Complexation of trivalent rare earth elements (Ce, Eu, Gd, Tb, Yb) by carbonate ions. Geochim. Cosmochim. Acta 57, 295–302.

Masuda, M., Ikeuchi, Y., 1979. Lanthanide tetrad effect observed in marine environment. Geochem. J. 13, 19–22.

Masuda, A., Kawakami, O., Dohmoto, Y., Takenaka, T., 1987. Lanthanide tetrad effects in nature: two mutually opposite types, W and M. Geochem. J. 21, 119–124.

Maynard, J.J., Anderson, M.A., Green, S., Graham, R.C., 1994. Physical and hydraulic properties of weathered granitic rock in Southern California. Soil Sci. 158, 375–380.

McLennan, S.M., 1989. Rare earth elements in sedimentary rocks: influence of provenance and sedimentary processes. Rev. Mineral. 21, 169–200.

McLennan, S.M., 1994. Rare earth elements geochemistry and the "tetrad effect". Geochim. Cosmochim. Acta 58, 2025–2033.

McLennan, S.M., Taylor, S.R., 1979. Rare earth element mobility associated with uranium mineralization. Nature 282, 247–250.

Minami, M., Matsuda, N., Masuda, A., 1995. Experimental studies on behaviors of lanthanides in interaction between water and basaltic rock grains. Proc. Jpn. Acad. 71 (B), 10–14.

Mizutani, Y., Seo, T., Ota, K., Nakai, N., Murai, Y., 1992. Carbon-14 ages of deep groundwater from the Tono uranium mine, Gifu, Japan. Proc. Symp. on Accelerator Mass Spectrometry and Interdisciplinary Application of Carbon Isotopes, 159–168 (in Japanese with English abstract).

Möller, P., Bau, M., 1993. Rare-earth patterns with positive cerium anomaly in alkaline waters from Lake Van, Turkey. Earth Planet. Sci. Lett. 117, 671–676.

Nesbitt, H.W., 1979. Mobility and fractionation of rare earth elements during weathering of a granodiorite. Nature 279, 206–211.

Nesbitt, H.W., Young, G.M., 1982. Early Proterozoic climates and plate motions inferred from major element chemistry of lutites. Nature 299, 715–717.

Ochiai, Y., Takeda, S., Yanagida, K., Nakatsuka, N., 1989. Natural analogue study on uranium deposit in Japan. Proc. Third CEC Natural Analogue Deposit in Group Meeting. CEC Report No. EUR11725EN, pp. 126–138.

Ohta, A., Kawabe, I., 2000. Theoretical study of tetrad effects observed in REE distribution coefficients between marine Fe–Mn deposit and deep seawater, and in REE(III)–carbonate complexation constants. Geochem. J. 34, 455–473.

Peppard, D.F., Mason, G.W., Lewey, S., 1969. A tetrad effect in the liquid–liquid extraction ordering of lanthanide(III). J. Inorg. Nucl. Chem. 31, 2271–2272.

Sano, Y., Terada, K., Nishio, Y., Amakawa, H., Nozaki, Y., 1999. Ion microprobe analysis of rare earth element in oceanic basalt glass. Anal. Sci. 15, 743–748.

Sano, Y., Hidaka, H., Terada, K., Shimizu, H., Suzuki, M., 2000. Ion microprobe U–Pb zircon geochronology of the Hida gneiss: finding of the oldest minerals in Japan. Geochem. J. 34, 135–154.

Shinotsuka, K., Hidaka, H., Ebihara, M., Nakahara, H., 1996. ICP-MS analysis of geological standard rocks for yttrium, lanthanoids, thorium and uranium. Anal. Sci. 12, 917–922.

Sholkovitz, E.R., 1988. Rare earth elements in the sediments of the

North Atlantic Ocean, Amazon Delta, and East China Sea: reinterpretation of terrigenous input patterns to the oceans. Am. J. Sci. 288, 236–281.

Smedley, P.L., 1991. The geochemistry of rare earth elements in groundwaters from Carnmenellis area, southwest England. Geochim. Cosmochim. Acta 55, 2767–2779.

Stetzenbach, K.J., Amano, M., Kreamer, D.K., Hodge, V.F., 1994. Testing the limits of ICP-MS: determination of trace elements in ground water at the part-per-trillion level. Ground Water 32, 976–985.

Stumm, W., Morgan, J.J., 1996. Aquatic Chemistry, 3rd edn. Wiley, New York.

Suzuki, K., Adachi, M., 1998. Denudation history of the high T/P Ryoke metamorphic belt, southwest Japan: constraints from CHIME monazite ages of gneisses and granitoids. J. Metamorphic Geol. 16, 23–37.

Takahashi, Y., Shimizu, H., Kagi, H., Yoshida, H., Usui, A., Nomura, M., 2000. A new method for the determination of $Ce^{III}/Ce^{IV}$ ratios in geological materials; application for weathering, sedimentary, and diagenetic processes. Earth Planet. Sci. Lett. 182, 201–207.

Taylor, S.R., McLennan, S.M., 1988. The significance of the rare earths in geochemistry and cosmochemistry. In: Gschneider, L., Eyring, L. (Eds.), Handbook on the Physics and Chemistry of Rare Earths, vol. 11. Elsevier, Amsterdam, pp. 485–580.

Toyoda, T., Nishi, S., Oki, T., Kuwahara, K., Ichikawa, K., Kutara, K., Hirano, I., 1999. A Guide to Draw Geological Column for Drilling Core (Bohring Chujyouzu Sakusei Yoryou Kaisetsusho). Japan Construction Information Center, p. 10 (in Japanese).

Yamamoto, I., Shiota, T., Harashima, F., Fujimoto, J., Koinuma, M., Hirono, S., 1974. Uranium exploration in the Tono district, Gifu Prefecture, Japan. Min. Geol. 24, 123–132.

Yanagisawa, K., Imai, H., Saito, A., Ohsawa, H., Nakajima, M., 1991. Analytical prediction of groundwater flow in the shaft excavation effect experiment. PNC Technical Report, GE 90-04.

Yoshida, H., 1994. Relation between U-series nuclide migration and microstructural properties of sedimentary rocks. Appl. Geochem. 9, 479–490.

Yoshida, H., Kodama, K., Ota, K., 1994. Role of microscopic flowpaths on nuclide migration in sedimentary rocks. A case study from the Tono uranium deposit, central Japan. Radiochim. Acta 66/67, 505–511.

Wood, S.A., 1990. The aqueous geochemistry of the rare-earth elements and yttrium: 1. Review of the available low-temperature data for inorganic complexes and inorganic REE speciation in natural waters. Chem. Geol. 82, 159–186.

Zhang, J., Amakawa, H., Nozaki, Y., 1994. The comparative behaviors of yttrium and lanthanides in seawater of the North Pacific. Geophys. Res. Lett. 21, 2677–2680.